

UCSF

UC San Francisco Electronic Theses and Dissertations

Title

Mechanisms of human neocortical expansion

Permalink

<https://escholarship.org/uc/item/8987n497>

Author

LaMonica, Bridget Elaine

Publication Date

2014

Peer reviewed|Thesis/dissertation

Mechanisms of human neocortical expansion

by

Bridget Elaine LaMonica

DISSERTATION

Submitted in partial satisfaction of the requirements for the degree of

DOCTOR OF PHILOSOPHY

in

Neuroscience

in the

GRADUATE DIVISION

of the

UNIVERSITY OF CALIFORNIA, SAN FRANCISCO

© Copyright (2014)

by

Bridget Elaine LaMonica

ii

This dissertation is lovingly dedicated to my dad, Frank LaMonica (1949-2004).

ACKNOWLEDGEMENTS

I am grateful to my advisor, Dr. Arnold Kriegstein, for accepting me into his laboratory and for providing thoughtful guidance and support. Arnold strikes a wonderful balance between giving his trainees freedom to pursue our interests, while always keeping his door open for discussion and advice. We have all benefitted immensely from his detailed knowledge of the field of developmental neuroscience, past and present. Also, the anecdotes he shares during lab meeting related to science politics are both informative and seriously amusing.

The Kriegstein lab would not have been the same without my fabulous lab mates, who together created a cooperative and welcoming lab environment. I am grateful to everyone in the lab for stimulating discussions of all types, for endless technical help and guidance, for coding my data with hilarious names so that I could perform blind quantifications, and for making lab meetings lively and enjoyable. In particular, I thank William Walantus for being the most accommodating and helpful lab manager anyone has ever had the pleasure of working with, and for letting me invade his workshop and use his power tools. I also thank Caitlyn Gertz, my lovely co-grad student, for joining me in the fight for healthful lab meeting food, and for the intermittent use of her name. To Cath Rottkamp, you are one of the most kindhearted and compassionate people that I know. Thank you for instructing me on the physical exam, and for your thoughtful career-related advice. Finally, I thank Jan Lui for sharing interesting imaris room podcasts, for being my older and wiser student mentor, and for helping me build and maintain my bikes. Jan has been more than just a great lab mate- he has been a wonderful friend (and big sister). I will sorely miss our impromptu swing dance lessons.

I am grateful to my neighbors in surrounding labs, who made HSW12 and Pod D friendly and collaborative places to work. In particular, I thank Ryan Delgado, Alex Ramos, and John Liu, for MSTP

love, in depth running discussions, and entertaining antics. I must also thank the MSTP community, including our administrators Jana and Catherine, who are seemingly capable of accomplishing anything. I thank the past and current MSTP directors, Drs. Kevin Shannon and Mark Anderson, for tireless support, advice, and witty comments. I am also grateful to the Neuroscience graduate program, particularly to the administrators Pat and Lucita, and to the past and current directors, Drs. Lou Reichardt and Roger Nicoll, for flexibility and for helping me navigate the grad school waters.

I am fortunate to have had many amazing mentors along my path to becoming a physician scientist (which is far from complete). I am grateful to my thesis committee, Drs. Arturo Alvarez-Buylla, David Rowitch, Erik Ullian, and David Hansen. Despite their busy schedules, they devoted ample time to discussing my research and providing comments on manuscripts. Their guidance greatly improved my projects and contributed to my scientific development. I am also grateful to my physician preceptors for patiently teaching me despite my seeming continual decrease in clinical knowledge. In particular, I thank Drs. Chris Fee, Andy Josephson, Dan Lowenstein, and Naomi Stotland for unending wisdom, clinical pearls, and words of encouragement. I also thank Drs. Nancy Sturm and David Campbell, in whose lab at UCLA I began my scientific training. I am grateful for their insistence on a rigorous understanding of basic molecular biology and minimal usage of pre-made kits. David and Nancy, thank you for providing me with the best scientific foundation possible, and for spoiling us with lab birthday parties. I am also deeply grateful to my mentor and advocate in the Campbell/Sturm lab, Dr. Robert Hitchcock. Bob, thank you for taking in an angsty freshman in highwater jeans, and for patiently coaching me in the ways of molecular biology. Thank you for the many nights of jamming in your garage (I miss your awesome slide guitar playing!), for your humor and sincerity, for support during difficult times of my life, and for simply being a true friend. I also cannot express the extent of my gratitude to Dr. Jonah Chan, a scientific and life mentor for almost a decade. Jonah's passion for scientific discovery and commitment to integrity are an inspiration. Jonah, thank you for your uncommonly thoughtful advice, realistic yet compassionate, about

some of the most important decisions of my life thus far. I would be in a much different place, scientific, geographic, and otherwise, without having known you.

I am grateful to my incredible family and friends, whose unyielding support made my scientific endeavors possible. I am forever indebted to my parents, Frank and Ruth, for unconditional love and almost unreasonably high expectations. My mom's strength and independence serve as an example worth striving for. I would have loved to share this accomplishment with my dad, a musical and mathematical genius who always told me to follow my dreams. I am grateful to my brilliant, beautiful, sisters, Lynette, Lauren, and Megan, to my preschool teacher and mentor Bill, and to my stepmom Arleen, for love and support throughout my life. I would also like to thank the Ostrems, in particular Cindy and Dennis, for being such a kind and welcoming second family to me. I also thank my friends at UCSF and elsewhere for encouraging my scientific pursuits, and for our lovely memories outside the lab. To my wonderful med school friends, especially Bogdana, Amanda, Didi, and Theresa: thank you for spa days, girls' nights, and for your kind and nonjudgmental support. Thank you to my MSTP classmates, in particular, Justin, Amanda, and Christina, for your friendship and camaraderie. I am also grateful to my ATX and LA friends, especially Maggie, Kate, and Melis, for their encouragement and love that has kept me going for years and years at all hours of the day and night.

Finally, I would like to thank my husband, Jonathan Ostrem, who supported me through all of the successes and failures of my PhD years. Jon, you are an unbelievably smart man whose kindness and humility are truly inspiring. Thank you for sharing your life with me.

CONTRIBUTIONS TO PUBLISHED WORK

All of the work described in this dissertation was done under the direct supervision and guidance of Arnold Kriegstein.

Parts of Chapters 1 and 4 are modified and reproduced from the review article: **LaMonica, B.E.**, Lui, J.H., Wang, X., and Kriegstein, A.R. OSVZ Progenitors in the human cortex: an updated perspective on neurodevelopmental disease. *Curr Opin Neurobio* 2012, 22: 1-7. This manuscript is reproduced in accordance with the policies of *Elsevier*. I created the figures and wrote the majority of the manuscript, with some sections written by Jan Lui and Xiaoqun Wang. Editing was performed by all authors.

Chapter 2 is reproduced from the publication: **LaMonica, B.E.**, Lui, J.H., Hansen, D.V., and Kriegstein, A.R. Mitotic spindle orientation predicts outer radial glial cell generation in human neocortex. *Nat Commun.* 2013;4:1665. This manuscript is reproduced in accordance with the policies of *Nature Publishing Group*. I am grateful to David Hansen for making the initial observation by time-lapse imaging of an approximately equal proportion of horizontal and vertical ventricular radial glial divisions in the human fetal neocortex. Supplemental Movie S1 was created by him. Based on this observation, I performed a quantitative analysis of cleavage angle of ventricular radial glia and outer radial glia, using further time-lapse imaging of slice culture, and immunohistochemistry of fixed cryosections. Jan Lui performed many of these experiments with me, and also assisted on analysis of outer radial glial morphology. I analyzed the cell-intrinsic nature of mitotic behaviors using dissociated cell culture, with immense help during the initial imaging sessions from Jiadong Chen. I generated the figures and wrote the manuscript, which was edited by all authors. This work was guided by Arnold Kriegstein.

Chapter 3 is a work in progress based largely on experiments that I designed after writing the manuscript that formed the basis for Chapters 1 and 4. I initially tested multiple cytoskeletal inhibitors in slice culture for effects on mitosis and mitotic somal translocation, and was surprised to find specific, reproducible effects that formed the basis for the rest of the study. Jan Lui provided invaluable assistance during the preliminary experiments, and also during subsequent imaging sessions, particularly when slice culture was involved. Caitlyn Gertz performed all experiments involving ferret tissue. I generated the figures and wrote the manuscript, which was edited by all authors. This work was guided by Arnold Kriegstein.

The manuscripts that form Chapters 2-3 benefitted greatly from the critical reading and insightful comments of Arturo Alvarez-Buylla and Jonah Chan.

Mechanisms of human neocortical expansion

By Bridget Elaine LaMonica

ABSTRACT

One of the most remarkable features of human brain evolution is the enormous increase in neuron number and the transformation of the lissencephalic cortex into a highly folded gyrencephalic cortex. Neocortical expansion is thought to both underlie the unique cognitive abilities of humans, and to result in certain disease susceptibilities. The massive increase in neurons in the human brain is established primarily by large numbers of a specific type of neural stem cell present during fetal development, the outer radial glial (oRG) cell. In the few years since their initial description, these cells have become the focus of intense interest because of their role in brain expansion and evolution. However, the developmental origins of oRG cells, and the mechanisms regulating their proliferation, are unknown. In this thesis, I describe our efforts to understand the unique role of oRG cells in human brain evolution. Using time-lapse imaging of human fetal cortical slices, we find that oRG cells are progeny of ventricular radial glial (vRG) cells, the primary neural stem cell present in all mammals. We further observe that vRG cell mitotic spindle angle determines daughter cell fate. Horizontal divisions, which are far more common in human than in mouse, lead to oRG cell generation, while vertical divisions do not. These results suggest that an increase in horizontal vRG divisions might have expanded the oRG cell population during primate brain evolution.

We next use dissociated human fetal cortical cultures, in conjunction with a panel of chemical inhibitors, to explore the molecular pathways regulating oRG cell division. During a process called mitotic somal translocation (MST) that occurs immediately before cytokinesis, the oRG cell body rapidly translocates a distance of several cell diameters towards the cortical plate. We find that oRG cell MST and cleavage

angle regulation are cell intrinsic. Activation of the Rho effector ROCK and of non-muscle myosin II, but not microtubule polymerization or centrosomal guidance, are required for MST. MST is independent of mitosis, and mechanistically distinct from vRG cell interkinetic nuclear migration and neuronal migration. Furthermore, oRG cell MST at the basal border of the oSVZ leads to radial oSVZ expansion. We propose that MST may have evolved to reduce cell crowding and minimize ventricular surface area by promoting radial over tangential progenitor zone expansion. MST may also serve to accelerate fetal brain development by delivering oRG daughters, including intermediate progenitor cells and their neuronal progeny, closer to their destinations in the cortical plate.

Finally, we describe several genetic mutations that target the RhoA-ROCK-myosin II pathway and cause cortical malformations in humans, including microcephaly, periventricular heterotopia, and lissencephaly. These malformations have largely been attributed to defective neuronal migration, but our finding that ROCK and myosin II activation are necessary for MST suggests that MST may also play a role in the etiology of these disorders. Further evidence comes from the expression patterns within the fetal human cortex of several candidate genes, which resemble the expression patterns of known oRG genes more closely than the expression patterns of neuronal genes. We note that many of the mutations involving ROCK and myosin II that are associated with dramatic human cortical malformations produce very minimal phenotypes in mice. We propose that MST may be the primary target of these diseases, as oRG cells comprise a very small proportion of neural progenitor cells in mice. Given our discovery of the origin of oRG cells and the molecular motor driving MST, the field will now be in a better position to understand the function of oRG cells and oRG-specific behaviors such as MST in human brain development and disease.

TABLE OF CONTENTS

Chapter 1	Introduction	1
Chapter 2	Mitotic spindle orientation predicts outer radial glial cell generation in human neocortex	13
Chapter 3	Control of outer radial glial cell mitosis and progenitor zone expansion in the human brain	45
Chapter 4	Concluding Remarks and Future Work	86
Chapter 5	References	90

LIST OF TABLES

Chapter 3

Supplementary Table 1	Mutations in genes that regulate the RhoA-ROCK-Myosin II pathway.	76
----------------------------------	---	----

LIST OF FIGURES

Chapter 1

Figure 1	Increased spatial and cellular complexity of the developing human cortex.	10
Figure 2	Molecular mechanisms of centrosome and microtubule-related cell behaviors in the developing neocortex.	11

Chapter 2

Figure 1	Horizontal vRG divisions produce oRG cells.	27
Figure 2	oRG cells divide horizontally to self-renew.	29
Figure 3	Apical and basal processes on oRG cells and oRG apical daughters.	31
Figure 4	Dissociated cortical progenitor cells display MST and horizontal spindle orientation.	33
Figure 5	MST and establishment of a horizontal spindle orientation are cell-intrinsic processes.	34
Figure 6	Model of cleavage angle regulation of cell fate during human cortical development.	36
Supplementary Figure S1	Composition of primary dissociated cortical progenitor cultures.	38
Supplementary Movie S1	vRG cells dividing at ventricular surface.	39
Supplementary Movie S2	Horizontal vRG divisions produce oRG cells.	39
Supplementary Movie S3	oRG cells divide horizontally to self-renew	39
Supplementary Movie S4	INM-like behavior in dissociated cells.	39
Supplementary Movie S5	Symmetrical oRG cell division.	40

Chapter 3

Figure 1	oRG cell MST requires myosin II but not microtubule motors.	56
Figure 2	Dissociated human cortical progenitor cells express oRG cell markers and require myosin II for MST.	57
Figure 3	Role of microtubules and the centrosome in MST.	59
Figure 4	MST promotes developmental oSVZ expansion and delivery of committed neural precursors closer to the cortical plate.	61
Supplementary Figure S1	Experimental setup.	63
Supplementary Figure S2	Expression of non-muscle myosin II (NMII) in fetal human cortex.	65
Supplementary Figure S3	Rare oRG daughters in dissociated culture express Tbr2.	67
Supplementary Figure S4	Wash-out of nocodazole results in division of oRG cell that previously underwent MST without cytokinesis.	68
Supplementary Figure S5	Inhibitor treatment does not induce apoptosis.	69
Supplementary Figure S6	Dsred-Cent2 construct labels centrosomes.	71
Supplementary Figure S7	oRG basal fiber contraction during MST.	72
Supplementary Figure S8	Frequency of MST is increased in human as compared to ferret cortex.	73
Supplementary Figure S9	Expression in germinal zones of the fetal human brain of genes associated with both the RhoA-ROCK-NMII pathway and developmental cortical malformations in humans.	74

CHAPTER 1

Introduction

The human neocortex has undergone a marked expansion as compared to other vertebrate species (Lui 2011; Lamonica 2012). Recent studies have begun to uncover unique features of the fetal primate brain that may account for its increased size and neuronal number (Smart 2002; Fietz 2010; Hansen 2010; Martinez-Cerdeno 2012). While both the developing primate and rodent brains contain a ventricular zone populated by neural stem cells called ventricular radial glial (vRG) cells (Rakic 1971; Pixley 1984; Hockfield 1985; Bentivoglio 1999), the primate neocortex displays an additional region of neurogenesis that is absent in rodents; the outer subventricular zone (oSVZ) (Smart 2002; Zecevic 2005; Hansen 2010) (Figure 1). The oSVZ is located at a distance from the ventricle and contains a large number of outer RG (oRG) cells, neural stem cells that express vRG markers but display characteristics distinct from vRG cells. oRG cells appear to contribute to human neocortical expansion by increasing the absolute number of neuronal progenitor cells, and by giving rise to more neuronal progeny per progenitor cell, through a process termed "transit amplification" (Lui 2011). As oRG cells make up a large proportion of progenitor cells in developing human but not mouse cortex (Wang 2011), it has been hypothesized that genetic mutations causing dramatic cortical malformations in humans, but minimal phenotypes in mouse, preferentially affect oRG cells. However, the mechanisms regulating oRG cell production and proliferation are unknown, hindering exploration of a potential role for oRG cells in human disease.

Neural progenitors in the rodent neocortex

During embryonic development, excitatory neurons of the mammalian neocortex originate from a proliferative epithelium of vRG cells that line the cerebral ventricles (Kriegstein 2009) (Fig. 1a). Much of our understanding of the events intervening between vRG cell proliferation and neuronal production is based on rodent studies, where vRG cells are primarily restricted to the ventricular zone (VZ) and undergo multiple rounds of asymmetric divisions to both self-renew and produce intermediate progenitor (IP) cells. While vRG cells display the apical-basal polarity typical of a neuroepithelium, IP cells appear to lack apical-basal polarity. IP cells subsequently occupy the subventricular zone (SVZ) and divide

symmetrically to generate neurons that migrate along vRG fibers towards the pia, populating the cortical plate (Noctor 2004). Because vRG cells primarily undergo asymmetric self-renewing divisions, and IP cells primarily undergo only one round of transit-amplifying division to produce two neurons, neurogenesis in the rodent involves a stable-sized population of progenitor cells bordering the lateral ventricles (Haubensak 2004; Miyata 2004).

In order for these events to unfold, a number of important cell movements must be properly regulated. First, vRG cells exhibit a highly stereotyped behavior known as interkinetic nuclear migration (INM), where the cell body shuttles up and down in the VZ in coordination with its cell cycle phase. The nucleus ascends to the upper VZ during G1 phase, and after passing through S phase descends during G2 to undergo M phase at the ventricular surface (Taverna 2010). vRG cells also control their cleavage plane such that the self-renewed cell retains both apical and basal membrane, whereas the daughter cell delaminates from the epithelial structure to become an IP cell. Finally, once neurons are born in the SVZ, they must be able to migrate long distances in the radial direction, towards the cortical plate (Noctor 2004).

Current molecular understanding of neurodevelopmental diseases

Much of our current understanding of human disease came from combining knowledge of human genetics with mouse models. Cell cycle regulation, neurogenesis, and the origin of human developmental diseases were linked by the identification of genes associated with cortical malformations such as microcephaly and lissencephaly (Manzini 2011). Many of these genes encode centrosomal and microtubule-related proteins important for cell division (neurogenesis), migration, and/or other dynamic behaviors such as INM. This observation merits a brief discussion of centrosome and microtubule functions in INM, mitosis, and neuronal migration in the developing neocortex.

INM precedes mitosis in vRG cells and involves the centrosome and microtubule-based motors, as well as the actomyosin system (Taverna 2010) (Fig. 2a,b). During the G1 phase of INM, apical-to-basal nuclear movement is directed away from the centrosome, which is located at the base of the primary cilium, at the most apical pole of the cell. Microtubules are oriented parallel to the apical-basal axis with the minus ends closer to the ventricle. Plus-end-directed motor proteins (kinesins), such as KIF1A, are involved in pulling the nucleus in a basal direction (Taverna 2010; Tsai 2010). The actomyosin motor system is also involved in apical-to-basal INM, as myosin II inhibition selectively retards this phase of INM in mouse cortex (Schenk 2009). During G2, basal-to-apical nuclear movement is directed toward the centrosome. The minus end-directed motor protein dynein, and the dynein-interacting protein LIS1, control basal-to-apical nuclear movements during INM (Tsai 2007; Tsai 2010), and the microtubule-associated protein TPX2 moves into the apical process from the nucleus during this phase, further modulating microtubule dynamics (Kosodo 2011). Recent studies examining the role of the actomyosin motor system in basal-to-apical INM have shown that this behavior is specifically affected by inhibition of the small GTPase Rac in developing mouse brain (Minobe 2009), or by myosin II inhibition in zebrafish retina (Norden 2009). These findings suggest that the degree to which actomyosin motors contribute to basal-to-apical INM is not completely clear and may be species-specific. As M phase proceeds, the centrosome continues to play important roles as both the location of checkpoint proteins and a physical organizer of cell division (Fig. 2c). The G2 to M transition involves centrosome-mediated microtubule nucleation (Zimmerman 2004). The centrosome during metaphase organizes the spindle and microtubule attachment to kinetochores, and the centrosome further functions in cytokinesis and mitotic exit (Doxsey 2005). Differential inheritance of mother and daughter centrosomes suggests that these organelles also play a role in asymmetric inheritance of cellular components and subsequent determination of daughter cell fates (Yamashita 2007; Wang 2009).

After vRG cells divide at the VZ, newborn cortical neurons migrate to the cortical plate along vRG fibers (Fig. 2d). The two main dynamic events during neuronal locomotion are leading process growth and

nucleokinesis. Centrosome movement into the leading process precedes nucleokinesis, and a microtubule lattice originating from the centrosome surrounds the nucleus and forms a cage that functions to pull the nucleus up into the leading process (Huang 2009). The dynein complex, including the regulatory protein LIS1, controls centrosome movement into the leading process, and coupling of centrosomal and nuclear movements (Tsai 2007). Doublecortin (DCX), another microtubule-binding protein, has also been implicated in radial neuronal migration (Bai 2003; Koizumi 2006).

A clear indication that mutation of centrosomal proteins can cause defects in neurogenesis came from identification of the genes responsible for autosomal recessive primary microcephaly (MCPH) in humans. Five of the eight known MCPH genes encode proteins that localize to the centrosome during all or part of the cell cycle: microcephalin (*McpH1*) (Jackson 1998; Jackson 2002), centromere-associated protein J (*Cenpj*) (Leal 2003; Bond 2005), abnormal spindle-like microcephaly-associated protein (*Aspm*) (Pattison 2000; Bond 2002; Shen 2005), cyclin-dependent kinase 5 regulatory-associated protein 2 (*Cdk5rap2*) (Moynihan 2000; Bond 2005), and the pericentriolar gene *Stil* (Kumar 2009). This disease is characterized by a decrease in brain volume with grossly normal brain architecture, and patients can display various neurological and psychiatric features including seizures (most common), mental retardation, delayed motor and speech function, hyperactivity and attention deficit disorders, and balance and coordination difficulties (Kaindl 2009). Mouse models have indicated that ASPM is involved in maintaining symmetric divisions of vRG cells, and may be involved in completion of cytokinesis (Kouprina 2005; Fish 2006; Higgins 2010). In the mouse brain, CDK5RAP2 is highly expressed in the neural progenitor pool, and its loss results in a depletion of vRG cells and increased cell-cycle exit leading to premature neuronal differentiation (Megraw 2011). This protein has also been shown to stimulate microtubule nucleation (Choi 2010) and regulate centriole replication (Barrera 2010). CDK5RAP2 function was linked to the pericentriolar protein, pericentrin, as depletion of pericentrin in neural progenitor cells phenocopies the effects of CDK5RAP2 knockdown and results in decreased recruitment of CDK5RAP2 to the centrosome (Buchman 2010). Similar to MCPH genes, pericentrin mutation in

human patients causes reduced brain and body size (Rauch 2008). Microdeletions encompassing human *Nde1*, also a centrosomal gene, are risk factors for microcephaly, mental retardation, and epilepsy (Ghannad 2011). Mutations in *Nde1* can also result in a condition called microlissencephaly, characterized by extreme microcephaly and grossly simplified cortical gyral structure (Alkuraya 2011). *Nde1* mutant mice displayed microcephaly, in addition to dramatic defects in mitotic progression, mitotic orientation, and mitotic chromosome localization in vRG cells, and altered neuronal cell fates. Mutated NDE1 protein was found to be unstable, incapable of binding cytoplasmic dynein, and had aberrant centrosomal localization (Feng 2004; Alkuraya 2011; Bakircioglu 2011). Other centrosome-associated proteins implicated in neurodevelopmental disease include WDR62, which causes microcephaly with simplified gyri and abnormal cortical architecture (Bhat 2011), and CEP152, the putative mammalian ortholog of *Drosophila* *asterless* which affects mitosis in the fly and results in primary microcephaly in humans (Guernsey 2010).

Defects in microtubules and associated proteins have primarily been hypothesized to affect dynamic cellular processes such as INM and neuronal migration. Mutation of *Lis1* causes lissencephaly in the human brain, while knockdown of *Lis1* in rodents causes arrest of centrosomal and nuclear movements during neuronal migration, and disruption of basal-to-apical INM (Tsai 2007). Furthermore, knockout of *Lis1* in neural progenitors disrupts regulation of vRG cleavage plane angle, leading to widespread apoptosis of neuroepithelial cells and culling of the progenitor pool (Yingling 2008). This phenotype results from an inability of astral microtubules to be captured by the cell cortex, leading to a failure of cell division. Tubulin-related disorders likely affect similar cellular processes; for example, mutations in alpha and beta tubulins, probably in domains necessary for microtubule polymerization or association with motor proteins, can cause severe lissencephaly and microcephaly in human patients, among other malformations (Tischfield 2011). In a mouse model of tubulin diseases, a mutation in *Tubal1* affecting tubulin heterodimer formation was shown to cause defective cortical lamination and neuronal migration

in mice (Keays 2007). It is thought that neuronal migration is similarly disrupted in humans with tubulin mutations.

The increased cellular complexity of human neocortical development

Recent studies have revealed an increased complexity in progenitor zone composition and structure in the developing human dorsal cortex as compared to rodents (Fietz 2010; Hansen 2010; Lui 2011; Betizeau 2013; Pilz 2013) (Fig. 1b). We must consider these differences when applying knowledge of the molecular mechanisms of disease in mice to our understanding of disease mutations in humans. The human neocortex, like the mouse and rat, also begins its development from an epithelium of vRG cells. However, the lineage relationship between human vRG cells and neurons is much more protracted than in the mouse, due to the process of transit amplification, resulting in an accumulation of progenitor cells before neuronal differentiation (Lui 2011). Most notably, there is an expanded proliferative region termed the oSVZ in the developing human neocortex that contains the majority of progenitor cells during peak periods of neurogenesis (Fietz 2010; Hansen 2010).

Unlike the rodent SVZ, which contains primarily IP cells, the human oSVZ contains cells that display diverse morphologies and that may express IP cell markers, vRG cell markers, or markers of both cell types (Hansen 2010; Betizeau 2013; Pilz 2013). In particular, recent studies have focused on a novel class of neural stem cell found in the oSVZ termed oRG cells. oRG cells express all known molecular markers of vRG cells. Timelapse imaging and fate analysis in human show that oRG cells can self-renew, expanding the oRG cell population, and can also give rise to an extended lineage of transit amplifying IP cells (Hansen 2010). Unlike vRG cells, oRG cells are located far from the ventricle, with no apical contact to the luminal surface, but they possess a long basal fiber that often extends to the pial surface. Similar but less numerous oRG and oRG-like cells have recently been characterized in other species, including mouse (Shitamukai 2011; Wang 2011), ferret (Fietz 2010; Reillo 2011; Reillo 2011; Gertz

2014) and marmoset (Garcia-Moreno 2012; Kelava 2012). oRG cells in mice were shown to be the progeny of vRG cells, suggesting a similar lineage relationship in humans (Shitamukai 2011; Wang 2011).

While vRG cells in the VZ undergo INM during mitosis, oRG cells undergo mitotic somal translocation (MST), a distinctive behavior where the cell soma rapidly ascends along its own radial fiber toward the cortical plate (CP) a distance of several cell diameters during the hour before cytokinesis (Hansen 2010; Wang 2011). The MST of oRG cells contrasts with the INM of vRG cells, in which the nucleus moves apically and mitosis occurs at the ventricular surface (Taverna 2010). However, the direction of nuclear movement just before cytokinesis is toward the centrosome in INM (Taverna 2010), and recent evidence in the mouse suggests that the centrosome moves into the leading process before nuclear translocation during MST (Wang 2011). It is therefore possible that the two behaviors involve conserved gene function (Fig. 2e). oRG cells use multiple rounds of cell division involving MST to simultaneously amplify neuron number and extend the boundary of the OSVZ outwards (Lui 2011). Both INM and MST differ from the far less dynamic IP cell mitosis, where the cell divides in place without nuclear translocation (Noctor 2004).

In this thesis, I describe our efforts to determine the origins of oRG cells in humans, and to uncover the mechanisms regulating oRG cell proliferation. Our approach centers on time-lapse imaging of human fetal brain tissue and dissociated progenitor cells. Our results demonstrate that vRG cells produce oRG cells, and that the angle of cell division determines daughter cell fate. We examine the cell-intrinsic properties of oRG cell MST and mitosis, and find that MST is driven by the Rho-ROCK-myosin pathway. We also explore centrosome dynamics and the role of microtubule motors during oRG cell division. Finally, we find that MST is required for progenitor zone expansion during human dorsal cortical development. Our findings help to fill a gap in our understanding of the cellular basis for

neocortical expansion. Furthermore, this thesis represents an essential first step in understanding the function of MST in human brain development and disease.

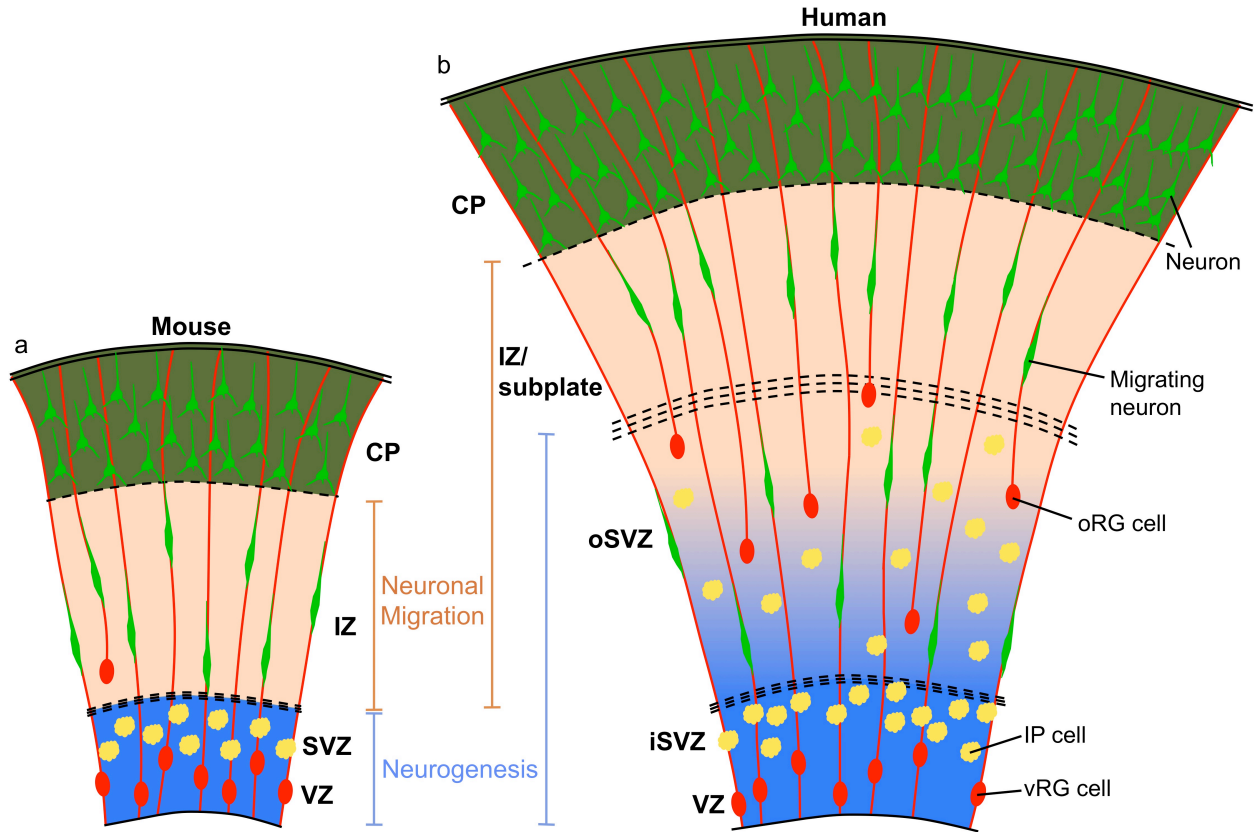


Figure 1. Increased spatial and cellular complexity of the developing human cortex. (a) Current model of mouse neocortical development. Primary zones of neurogenesis (blue) are the VZ and SVZ, where vRG cells and IP cells reside, respectively. Neurons born in the VZ or SVZ migrate along the vRG radial fiber scaffold found in the intermediate zone (IZ), the primary zone of neuronal migration (orange) in the mouse, to reach the cortical plate (CP). oRG cells are infrequent and not located in a distinct progenitor zone. **(b)** Expanded model of human neocortical development. vRG cells, IP cells, and oRG cells are found in neurogenic zones (blue), which are the VZ, the inner SVZ (iSVZ), and the outer SVZ (oSVZ). Neurons migrate through the oSVZ and IZ/subplate (zones of migration, orange) to populate the CP. Neurons must navigate a larger distance than in the mouse, and a radial fiber scaffold of increased complexity, to reach the CP.

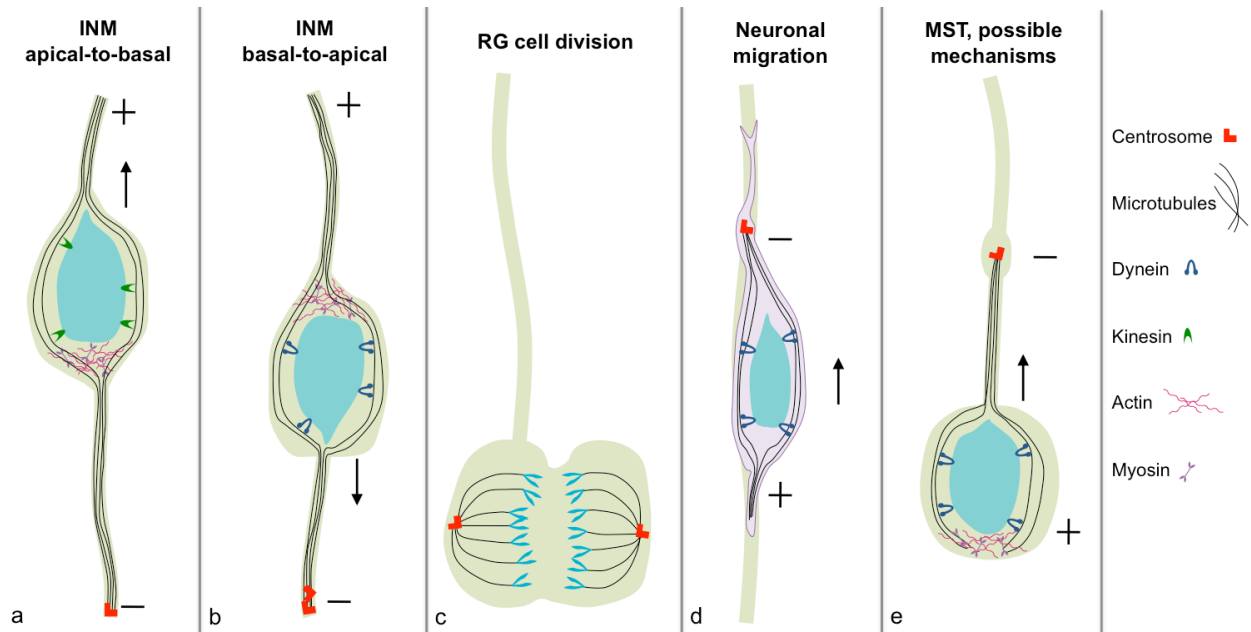


Figure 2. Molecular mechanisms of centrosome and microtubule-related cell behaviors in the developing neocortex. (a) A vRG cell is depicted undergoing apical-to-basal INM during the G1 phase of the cell cycle. The basal direction is up, apical is down, and the centrosome (red) is located at the ventricular surface at the base of the primary cilium (not shown). Kinesin and actomyosin motors control nuclear movement, which is ab-centrosomal and toward the microtubule plus ends. (b) vRG cell undergoing basal-to-apical INM during the G2 phase of the cell cycle. Nuclear movement is ad-centrosomal and towards microtubule minus ends. The process is controlled by dynein and associated proteins such as Lis1, and possibly by actomyosin motors. The centrosome has already replicated at this time. (c) vRG cell division at the ventricular surface. The centrosomes move to opposite poles of the cell and function throughout mitosis in microtubule nucleation, spindle and microtubule attachment to kinetochores, cytokinesis, and mitotic exit. The centrosome also plays a role in asymmetric inheritance of cell fate components in daughter cells. (d) Radial neuronal migration along a vRG fiber. The centrosome moves into the leading process prior to nucleokinesis, and a microtubule lattice originating from the centrosome forms a cage around the nucleus. Dynein and associated proteins function to pull the nucleus into the leading process. (e) oRG cell mitotic somal translocation (MST) is depicted with possible

molecular mechanisms controlling this cell behavior. Previous evidence suggests that the centrosome precedes the nucleus into the basal process, which leads to nuclear movement toward microtubule minus ends. MST may therefore utilize minus-end directed motors such as dynein, and/or actomyosin motors.

CHAPTER 2

Mitotic spindle orientation predicts outer radial glial cell generation in human neocortex

The content of this chapter was modified from the following publication:

LaMonica, B.E., Lui, J.H., Hansen, D.V., and Kriegstein, A.R. Mitotic spindle orientation predicts outer radial glial cell generation in human neocortex. *Nat Commun.* 2013;4:1665.

SUMMARY

The human neocortex is increased in size and complexity as compared to most other species. Neocortical expansion has recently been attributed to protracted neurogenesis by outer radial glial (oRG) cells in the outer subventricular zone (oSVZ), a region present in humans but not in rodents. The mechanisms of human oRG cell generation are unknown, but are proposed to involve division of ventricular radial glial (vRG) cells; neural stem cells present in all developing mammals. Here we show that human vRG cells produce oRG cells and seed formation of the oSVZ via horizontal divisions, which occur more frequently in humans than in rodents. We further find that oRG cell mitotic behavior is cell intrinsic, and that the basal fiber, inherited by oRG cells after vRG division, determines cleavage angle. Our results suggest that altered regulation of mitotic spindle orientation increased oRG cell numbers, and ultimately neuronal numbers, during human brain evolution.

INTRODUCTION

What cellular mechanisms led to an expanded oRG cell population and oSVZ size in the developing human brain? Evolutionary changes in mitotic spindle orientation could have altered the way cell fate determinants are segregated during vRG cell mitosis, affecting daughter cell fate and function and possibly leading to increased oRG cell generation. In vRG cells, cell fate determinants initially identified in *Drosophila melanogaster* neuroblasts associate preferentially with the apical domain or basal fiber (Chia 2008; Lui 2011; Lancaster 2012). These structures are differentially inherited in vRG daughter cells that subsequently display asymmetric fates (Peyre 2012). While localization of both progenitor (Bultje 2009; Zhang 2010) and neural (Zhong 1996; Shen 2002; Kusek 2012) fate determinants has been demonstrated at the apical domain, inheritance of the basal domain and fiber has been hypothesized as important for maintaining stem cell identity (Chenn 1995; Gaiano 2000; Fietz 2010; Fietz 2011; Lui 2011). In rodents, the majority of vRG divisions are oriented vertically, with a cleavage furrow perpendicular to the ventricular surface (Hinds 1971; Smart 1973; Landrieu 1979; Zamenhof 1987; Chenn 1995; Kamei 1998; Weissman 2003; Shitamukai 2011). During neurogenesis, one daughter inherits the basal fiber and half of the apical domain, becoming a self-renewed vRG cell. The other daughter inherits half of the apical domain, delaminates during the next cell cycle, and adopts a neuronal or IP cell fate (Noctor 2004; Shitamukai 2011). Interestingly, molecular perturbations that induce non-vertical cleavages in rodent vRG cells lead to the more basal daughter inheriting the basal fiber but no part of the apical domain, and adopting oRG-like morphology (Shitamukai 2011). These experiments suggest a possible evolutionary mechanism for increasing oRG cell generation in the fetal human brain.

During early brain development (prior to gestation week 10), the majority of vRG divisions in human cortex are vertically oriented (Howard 2006), but studies of mitotic spindle regulation in specific progenitor cell types during oSVZ formation and oRG production have been extremely limited. We

wanted to test whether regulation of mitotic spindle orientation is altered in fetal human neocortex during peak neurogenesis, when the oSVZ appears, and whether this leads to increased oRG cell production. Here, we show that oRG cells in the developing human cortex are produced from vRG cells following division with a non-vertical cleavage orientation in which the basal daughter inherits the basal fiber and becomes the new oRG cell. We further show that the vast majority of oRG divisions display a horizontal cleavage plane, leading to oRG cell self-renewal by the daughter that inherits the basal fiber. We observe that cell-intrinsic mechanisms establish cleavage angle and control mitotic somal translocation (MST) (Hansen 2010), an oRG-specific mitotic behavior, in oRG-like cells in dissociated culture. An increase in non-vertical divisions of vRG cells may have contributed to the evolutionary expansion of the human neocortex by allowing large numbers of oRG cells to be generated, greatly increasing neural progenitor cell number. Furthermore, the tight regulation of mitotic spindle orientation in both vRG and oRG division increases the ways by which neurogenesis could be affected in diseases that disrupt cleavage angle regulation, such as lissencephaly and microcephaly (Fish 2006; Yingling 2008; Lizarraga 2010; Gruber 2011; Kitagawa 2011; Lamonica 2012).

RESULTS

Horizontal vRG divisions produce oRG cells

Expansion of the oRG cell population within the oSVZ coincides with peak neurogenesis in the developing human neocortex (Hansen 2010); however, the origin of oRG cells in the human is unknown. It was recently demonstrated that a very small population of oRG cells exists in the mouse and is generated from oblique divisions of vRG cells (Shitamukai 2011; Wang 2011). We hypothesized that human oRG cells are likewise generated from horizontal or oblique vRG cell divisions in which the newly generated oRG daughter inherits the basal fiber and no part of the apical membrane. We investigated this by performing time-lapse imaging of dividing vRG cells in gestation week 16 (GW16) through GW18 human cortical slices. We sparsely labeled cortical cells by infection with a CMV-GFP adenovirus (Adeno-GFP), and observed that vRG cells underwent interkinetic nuclear migration (INM) (Supplementary Movie 1), as previously described in other species (Noctor 2004). In contrast to the primarily vertically oriented divisions in mouse cortex, we observed a mix of divisions displaying vertical (60-90°), oblique (30-60°), and horizontal (0-30°) cleavage planes with respect to the ventricular surface. Of 70 observed divisions at the ventricular surface, 21 were vertical, 6 were oblique, and 43 were horizontal (Fig. 1g). While cell movement out of the imaging field and short imaging time windows sometimes precluded analysis of daughter cell fate after cell division, we observed 15 divisions that appeared to produce an oRG daughter cell as defined by rapid translocation away from the ventricular surface and maintenance of a basal fiber but no apical end foot (Supplementary Movie 2 and Fig. 1a, c). Nearly all (14/15) of these divisions were horizontal, while the remaining division was oblique. In 7 of these oRG-generating divisions, we observed that the apical daughter clearly began to regrow a basal fiber, suggesting a self-renewed vRG fate. Finally, we performed fate staining on 4 pairs of daughter cells after horizontal division, and observed that in all cases, the daughter cell that adopted oRG morphology

maintained Sox2 expression and did not express Tbr2, consistent with oRG and not IP cell fate, and the apical daughter cell was similarly Sox2+/Tbr2-, consistent with a self-renewed vRG fate (Fig. 1b). We concluded that non-vertical divisions produce oRG cells in fetal human cortex.

It has been shown that during rodent neurogenesis, the majority of vRG cell divisions at the VZ have vertical cleavage planes, after which both daughters inherit half of the apical domain (Shitamukai 2011). One daughter cell may subsequently delaminate from the VZ, presumably becoming a neuron or IP cell. We asked whether in human vRG cells, vertical cleavages also led to inheritance of a portion of the apical domain by both daughter cells. Similar to rodent cortex, in 100% (12/12) of vertical vRG divisions in which the apical domains were clearly visible before and after cell division, both daughter cells inherited a portion of the apical membrane (Fig. 1d). These results suggest that, in contrast to oblique and horizontal divisions, vertical vRG cell divisions do not produce oRG cell daughters. Instead, vertical divisions in human may be similar to those in rodent cortex, resulting in one self-renewed vRG cell, and one IP cell or neuron that subsequently delaminates.

Horizontal vRG divisions occur throughout oSVZ expansion

We next examined regulation of vRG cell mitotic spindle orientation over time from GW12-18, the period of peak neurogenesis in primate neocortex (Smart 2002; Lui 2011). The OSVZ is expanding in size throughout this period, and oRG cells are increasing in number (Hansen 2010). Since our analysis showed that oRG cells are produced by non-vertical divisions, we predicted that we would observe horizontal and oblique vRG cleavages throughout this period. We performed immunohistochemistry on fixed GW12, 14, 16, and 18 human fetal neocortical tissue samples. We used an antibody against phosphorylated vimentin (pVim) to mark cells in M phase and to identify vRG cells by their ventricular location and basal fiber, co-staining with an antibody against phosphorylated histone H3 (pH3) to visualize chromosomes during mitosis. We then analyzed mitotic spindle orientation of vRG cells in either anaphase or telophase at the

VZ (Fig. 1e, f). We found a small increase in the percentage of horizontal/oblique divisions throughout this time period, from 37.5% at GW12 to 50% at GW18 (n=35-60 cells in at least five different sections from each age, generated from at least two different tissue samples for each individual) (Fig. 1g). Vertical divisions had a corresponding decrease, from 62.5% at GW12 to 50% at GW18. These observations represent an increased proportion of vertical divisions as compared to results from time-lapse imaging of dividing vRG cells at GW16/18, where 69.2% of divisions were horizontal/oblique and 30.8% were vertical, possibly reflecting the influence of cell culture conditions or a slight disruption of the ventricular surface in slice culture. Our observation that a much higher proportion of non-vertical vRG divisions occurs in humans than has been reported in rodents (Hinds 1971; Smart 1973; Landrieu 1979; Zamenhof 1987; Kamei 1998; Weissman 2003; Shitamukai 2011), the large increase in oRG cells in humans as compared to rodents (Hansen 2010; Wang 2011), and the evidence we have presented here for the synchronous timing of non-vertical vRG divisions with oRG cell generation and oSVZ expansion (Hansen 2010), further support a role for non-vertical vRG division in oRG cell generation.

oRG cells divide horizontally to self-renew

Our results indicated that during non-vertical vRG division, inheritance of the basal fiber and failure to inherit the apical domain coincide with oRG cell generation. It has been previously demonstrated that oRG divisions are self-renewing, where the more basal daughter maintains oRG identity, and the more apical daughter adopts either oRG or IP cell fate, depending on whether a new basal fiber is generated (Hansen 2010). We asked whether oRG cells divide with a horizontal spindle orientation, thereby allowing the more basal cell to retain the oRG cell identity associated with the basal fiber. We first examined oRG cell divisions in organotypic slice culture, noting that cells underwent MST, a highly dynamic process during which the nucleus moves a distance of approximately 50 μ m in the basal direction along their basal fiber within a one-hour period prior to cytokinesis (Hansen 2010). Cell divisions appeared horizontally oriented, with the cleavage plane perpendicular to the basal fiber (Fig. 2a-c and

Supplementary Movie 3). While oRG cells do not contact the ventricular surface, we nonetheless observed that 27.5% of oRG cells displayed short apical processes of mean length 8.4 μ m (Fig. 3a, e). To determine how the spindle orientation of oRG divisions compared to vRG divisions, we quantified cleavage plane angles in fixed GW16 brain slices, identifying oRG cells in anaphase or telophase by their basal fiber, pVim reactivity, and pH3 staining of condensed chromatin (Fig. 2d, e). This analysis revealed that the majority (96.3%) of oRG divisions were non-vertical (horizontal or oblique). A significantly higher proportion of oRG divisions were oriented horizontally (82.0%) when compared to vRG divisions at the ventricular surface (29.7%) (Pearson's Chi-squared test, $p < .0005$) (Fig. 1e, 2h). Correspondingly, there were significantly fewer vertical oRG divisions (2.8%) as compared to vertical vRG divisions (56.8%) (Pearson's Chi-squared test, $p < .0005$). We concluded that horizontal spindle orientation is an actively regulated component of self-renewing oRG divisions.

Previously, it has been demonstrated that the apical daughters of oRG cell divisions may adopt an oRG cell fate, or may become IP cells, expressing Tbr2 and undergoing further transit amplifying divisions (Hansen 2010). We characterized the morphology of apical oRG daughters, observing that in the majority of divisions (97.5%), the apical daughter produced an apical process within one hour of MST, (Fig. 3e, f). Within one hour, only 20% of apical daughters displayed a basal process, though this number increased to 60% within 10 hours, after which no further cells were observed to grow a basal process (Fig. 3f, g). Thus, the majority of apical daughters of oRG division ultimately adopt a bipolar morphology, though it is not yet clear how this correlates with IP cell vs. oRG cell fate.

IP cells divide symmetrically with a random cleavage angle

The predominantly horizontal divisions of oRG cells exploit the intrinsic polarity of these cells to asymmetrically segregate the basal fiber, potentially along with unidentified cell fate determinants, into the self-renewing oRG daughter. We hypothesized that mitotic spindle orientation would be randomly

distributed in IP cells, which are morphologically symmetrical and produce daughter cells with symmetric fates (Noctor 2004). In contrast to vRG and oRG cells, which undergo INM and MST, respectively, IP cells retract their processes, round up, and divide in place (Fig. 2f). We quantified cleavage plane angles in GW16 cortex of IP cells in anaphase or telophase, using the nearest pVim⁺ radial fiber as a reference point, since the radial fiber scaffold is oriented perpendicularly to the ventricular surface (Rakic 1971). IP cells were identified by their location in the iSVZ or oSVZ, positive Tbr2 staining, and a lack of basal fiber by pVim staining (Fig. 2g). Unlike oRG cells, which are located in the same region but undergo predominantly horizontal divisions, IP cell cleavage angles appeared randomly distributed (Fig. 2h). Thus, it appears as though the molecular machinery that controls mitotic spindle orientation and basal fiber inheritance in oRG cells is not active in IP cells.

Horizontal divisions are cell-intrinsic in oRG-like cells

In the developing rodent cortex, contact with the pial surface does not appear necessary for vRG function (Haubst 2006). However, it is unknown whether oRG cell function requires signals from surrounding brain structures, such as through oRG cell basal process contact with the basal lamina or blood vessels. To determine whether MST and its associated horizontal spindle orientation required extrinsic directional cues or would persist outside of the native cortical environment, we dissociated fetal human neocortex, labeled cells using Adeno-GFP, and performed time-lapse imaging for up to 10 days. We found that 19% of cells displayed one process analogous to the basal process of oRG cells, 29% displayed two processes, 48% were multipolar, and 4% did not display any processes (Fig. S1). The "two-process" group likely also contained oRG cells, as 27% of oRG cells *in vivo* display a short apical process (Fig. 3e). In dissociated cortical progenitor cell cultures generated from two different ages of samples (GW14 and GW16), we observed that MST occurred in cells displaying one prominent process with or without a second, smaller process (Fig. 4a). Since MST appears to be an identifying behavior of oRG cells that has not been shown to occur in any other cell type in the developing brain, we called progenitor cells in

culture that displayed MST “oRG-like cells.” oRG-like divisions contrasted with symmetric, IP-like divisions, which were far more numerous and in which cells rounded up and divided in place (Fig. 4b). While we occasionally observed oscillatory behavior of bipolar cells reminiscent of INM (Supplementary Movie 4), we did not observe any unambiguous examples of INM. Furthermore, INM is defined based on the direction of cell movement with respect to structures extrinsic to the cell, such as the ventricular surface or adhesion belt, and our dissociated cultures lacked epithelial features that would normally be present *in vivo*, in slice cultures, or in neural rosettes. Thus, we were able to further investigate MST, but not INM, in dissociated cell culture.

We next wanted to determine how closely MST in dissociated culture resembled observations in slice culture. The majority of oRG-like divisions (85.7%) had a "horizontal" or orthogonal cleavage angle with respect to the basal fiber orientation (Fig. 5a). The mean MST distance was 72.6 μ m, similar to published observations of MST in oRG cells in slice culture (Hansen 2010) (Fig. 5b). Several oRG-like cells were observed to undergo divisions in which the daughter cell that did not inherit the basal fiber grew a basal fiber during the next cell cycle, adopting oRG-like morphology and subsequently undergoing MST and dividing (Supplementary Movie 5 and Fig. 5c). This corresponds to observations in slice culture, in which the more apical daughter after an oRG division can either grow a new basal fiber, thereby expanding the oRG population, or can begin expressing neuronal lineage markers and undergoing transit amplifying IP cell divisions (Hansen 2010). In some cases, daughter cells translocated in directions that were independent of the original direction of MST, and dependent only upon the location of the newly grown “basal” fiber. We concluded that MST and horizontal cleavage plane orientation, progenitor cell behaviors unique to oRG cells, persist outside of the native context of the developing neocortex. MST appears to be a cell-intrinsic process, and the basal fiber directs establishment of a horizontal spindle orientation. MST may require signaling factors such as mitogens from neighboring cells, but does not require a radial fiber scaffold, or cues derived from contact with the basal lamina, blood vessels, or meninges.

DISCUSSION

We present here a model by which horizontal divisions may have contributed to the evolutionary expansion of the human neocortex by increasing oRG cells and their neuronally committed progeny (Fig. 6). We show that during peak neurogenesis in human cortex, between 37.5% and 50% of vRG cell divisions have a non-vertical (horizontal or oblique) cleavage plane, leading to the more basal daughter inheriting the basal fiber but not the apical end foot and adopting an oRG cell fate. This represents a large increase over the mouse, in which fewer than 10% of vRG divisions are non-vertical (Hinds 1971; Smart 1973; Landrieu 1979; Zamenhof 1987; Chenn 1995; Kamei 1998; Weissman 2003; Shitamukai 2011). A recent study indicated that the majority of divisions at the ventricular surface of the fetal human brain display a vertical cleavage angle, but the authors did not take into account morphological criteria (presence of a basal fiber) to ensure that only vRG cells were analyzed (Fietz 2010). Other cell types, such as short neural precursors and IP cells, divide at the ventricular surface and may account for many of the vertical divisions observed by Fietz et al (Weissman 2003; Zecevic 2004; Gal 2006; Stancik 2010). What mechanisms might have been responsible for an increase in horizontal vRG divisions in humans? Interestingly, expression of a dominant-negative form of the spindle angle regulator LGN causes mouse vRG cells to display non-vertical cleavage angles and results in oRG-like cell production (Shitamukai 2011). Mutations in LGN or other spindle angle regulators could have led to an increase in non-vertical vRG divisions in developing human cortex. It is also possible that other mechanisms of oRG cell generation exist, such as direct delamination, and we may have failed to observe this in our slice cultures due to a small sample size or our gestational age of analysis.

In the oSVZ, we observed that 97.2% of oRG divisions were non-vertical, with more horizontal than oblique divisions, indicating active regulation of mitotic spindle orientation in oRG cells. In contrast, IP cell division appeared more random. Our results differ from those obtained by Fietz and colleagues, who

found that Pax6⁺ progenitors within the oSVZ display a random cleavage angle at GW14-16 (Fietz 2010). However, the authors did not define oRG cells based on presence of a basal fiber as we did, which is important given co-expression in the P0 ferret i/oSVZ of Tbr2 and Pax6 in approximately 38% of progenitor cells (Reillo 2011). We show here that in human fetal cortex, basal fiber inheritance is associated with oRG fate after horizontal vRG division, and oRG self-renewal after horizontal oRG division. Furthermore, oRG-like cells in dissociated culture undergo MST and maintain a horizontal cleavage plane during division. These observations suggest that the basal fiber could both orient oRG cell division and control stem cell function, possibly due in part to Integrin, Notch, and/or Retinoic Acid signaling through the basal fiber (Chenn 1995; Campos 2001; Siegenthaler 2009; Fietz 2010; Hansen 2010). The direction of MST in dissociated cultures was dependent on the orientation of the basal fiber, but not on the direction of MST in previous divisions. Therefore, secreted molecules or signals such as those mentioned above from glia, the basal lamina, the adjacent radial fiber scaffold, or other sources may direct the prolonged growth of newly generated oRG and vRG basal fibers *in situ*, and prevent prolonged growth of apical processes, so that MST normally proceeds in the basal direction.

The role of the apical domain is less clear than that of the basal fiber. Within the oSVZ, oRG cells do not express apical proteins found in vRG cells that are associated with retained stem cell function, such as Par3, ZO-1, or Prominin-1 (Fietz 2010). Similarly, we observed that after horizontal or oblique vRG divisions, the daughter that adopted oRG cell morphology did not inherit the apical domain. Since oRG cells are able to produce neurogenic IP cells (Hansen 2010), inheritance of the apical domain is not required for maintenance of neurogenic ability. The apical domain and adhesion belt appear to play a tethering role, allowing vRG cells to receive signals carried in the cerebrospinal fluid, maintaining the VZ as a neurogenic niche distinct from the i/oSVZ, and possibly directing vRG-specific behaviors, such as INM. We did not observe obvious INM in our dissociated cortical cultures, which may reflect the absence of an adherens junction belt present *in vivo*, in slices and at least partially in cultured neural rosettes (Curchoe 2012). It is possible that vRG cells that would have undergone INM were converted into oRG

cells in dissociated culture due to lack of apical tethering, and therefore displayed MST as a result of basal-fiber mediated signaling. A previous study showed that loss of NUMB in mouse vRG cells leads to delamination and displacement from the ventricular zone due to disruption of adherens junctions, but that a progenitor state is nevertheless maintained (Rasin 2007). This further supports a tethering role for the apical domain, and it is possible that the delaminated vRG cells either retained vRG identity or adopted oRG identity.

Recent studies have demonstrated the presence of oRG cells and an oSVZ in agoutis (gyrencephalic rodents), and in marmosets, which are near-lissencephalic primates (Garcia-Moreno 2012; Hevner 2012; Kelava 2012), indicating that oRG cells are necessary, but not sufficient, for a gyrencephalic brain. Contributing mechanisms could include an increase in the total number of oRG cell divisions dependent on the length of brain development, decreases in cell cycle length in neural progenitor cells in the fetal human brain, and further differences in regulation of mitotic spindle orientation. Additionally, while rodent IP cells divide one time to produce two neurons, human IP cells in the oSVZ undergo many rounds of division before producing neurons (Noctor 2008; Hansen 2010), suggesting that cortical expansion may be further explained by increased transit amplification of oRG-generated IP cells. Taken together, our experiments demonstrate that regulation of mitotic spindle orientation is a conserved mechanism across species and cell types in the developing brain for controlling the balance of progenitor cell and neuronal populations. In vRG cells specifically, an increase in horizontal divisions may have contributed to neocortical expansion and gyrification in species such as humans that display an oSVZ and a large oRG cell population.

ACKNOWLEDGMENTS

We thank Kriegstein laboratory members, J. Chan, and A. Ramos for thoughtful discussions and critical reading of the manuscript. We thank C. Harwell for retroviral production, J.W. Tsai for helping perform one of the slice culture experiments, J. Chen for helping perform the dissociated cell culture experiments, and W. Walantus, Y.Y. Wang, and S. Wang for other technical support. We thank F. Gage for GFP-retrovirus reagents. We thank the staff at San Francisco General Hospital for providing access to donated fetal tissue. The research was made possible by a grant from the California Institute for Regenerative Medicine (Grant Number TG2-01153). Additionally, this work was supported by the Bernard Osher Foundation and by award number R01NS075998 from the NINDS. The contents of this publication are solely the responsibility of the authors and do not necessarily represent the official views of CIRM or any other agency of the State of California, or of the NINDS or the NIH.

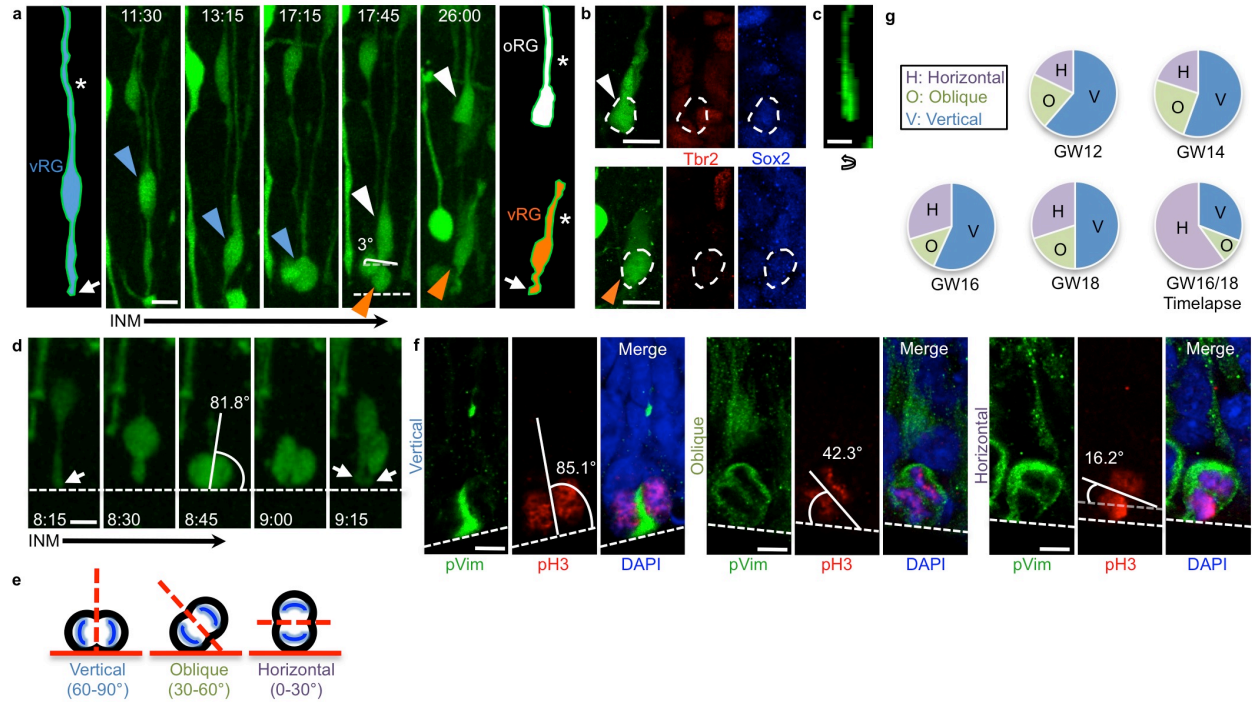


Figure 1. Horizontal vRG divisions produce oRG cells. a) Time-lapse stills of horizontal vRG division labeled with Adeno-GFP in GW16 human fetal cortical slice that results in generation of an oRG cell. vRG cell (blue arrowhead) starts at a distance from the ventricle, descends during interkinetic nuclear migration, and divides with a horizontal spindle orientation at the ventricular surface (dotted white line at 17:45). Basal daughter (white arrowhead) retains basal fiber (asterisk) and rapidly exits the ventricular zone, adopting oRG cell morphology. Apical daughter (orange arrowhead) inherits entire apical domain (white arrow) and regrows a basal fiber, becoming a self-renewed vRG cell. Cells of interest are schematized at beginning and end of sequence to more clearly demonstrate morphology and inheritance of basal fiber and apical domain. Scale bar, 10 μ m. **b)** Fate staining of daughter cells from division in (a) confirms that the basal daughter (white arrowhead) is Tbr2-/Sox2+, consistent with oRG identity, and the apical daughter (orange arrowhead) is also Tbr2-/Sox2+, consistent with vRG identity. Scale bar, 10 μ m. **c)** Z-plane analysis of basal daughter from division in (a) rotated 90° confirms lack of apical process. Scale bar, 10 μ m. **d)** Time-lapse stills of vertical vRG division in GW16 human fetal cortical slice after which both daughters inherit half of the apical domain (white arrows), and neither daughter adopts oRG morphology. Part of the basal fiber is not visible due to its location out of the imaged z-stack. Scale bar,

10 μ m. **e)** Schematic of vRG cells undergoing mitosis at the ventricular surface with vertical, oblique, and horizontal cleavage angles. Mitotic spindle orientation was analyzed with respect to the ventricular surface. **f)** Images of vRG cells in fixed human fetal cortical slices undergoing mitosis with vertical (left), oblique (center), and horizontal (right) mitotic spindle orientations at the ventricular surface. Scale bars, 5 μ m. **g)** Quantification of mitotic spindle orientation in fixed slices throughout peak neurogenesis and oRG cell generation, and during time-lapse imaging of GW16/18 human fetal cortical slices. Cells used for calculation in fixed slices were pH3⁺, pVim⁺ cells in anaphase or telophase that displayed a basal fiber and were located at the ventricular surface.

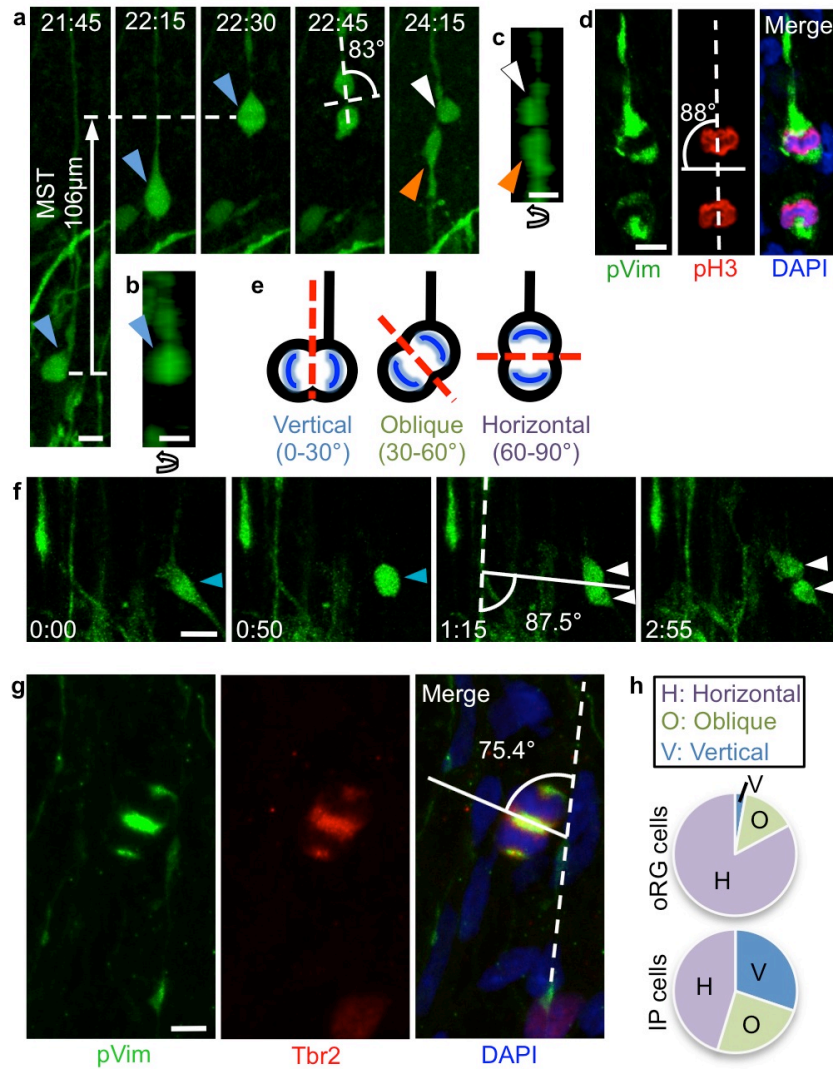


Figure 2. oRG cells divide horizontally to self-renew. **a)** Time-lapse stills of a dividing oRG cell (blue arrowhead) in GW16 human fetal cortical slice labeled with Adeno-GFP. The cell undergoes MST and divides with a horizontal spindle orientation, producing an apical daughter (orange arrowhead) and a basal daughter (white arrowhead). The basal daughter retains the basal fiber and becomes a self-renewed oRG cell, while the apical daughter produces an apical process. Scale bar 10 μ m. **b)** Z-plane analysis of oRG cell in first frame of (a), demonstrating lack of apical process. Scale bar, 10 μ m. **c)** Z-plane analysis of daughter cells in last frame of (a), demonstrating lack of apical process on basal daughter, and presence of apical process on apical daughter. Scale bar, 10 μ m. **d)** Image of oRG cell in fixed GW16 human fetal cortical oSVZ undergoing mitosis with a horizontal cleavage plane. Scale bar, 10 μ m. **e)** Schematic of

oRG cells undergoing mitosis with vertical, oblique, and horizontal cleavage planes. Cleavage plane angle was analyzed with respect to the basal fiber of the dividing cell (or in the case of IP cells, with respect to the nearest basal fiber). **f)** Time-lapse stills of IP cell (blue arrowhead) in a GW18 human fetal cortical slice that retracts its processes and rounds up to divide symmetrically, without undergoing MST or interkinetic nuclear migration, to produce two daughter cells (white arrowheads). Spindle orientation was calculated with respect to the nearest radial fiber. Scale bar, 20 μ m. **g)** Image of IP cell in fixed GW16 human fetal cortical oSVZ undergoing mitosis with a horizontal spindle orientation. Scale bar, 5 μ m. **h)** Quantification of mitotic spindle orientations in i/oSVZ progenitors (oRG cells and IP cells) in fixed GW16 human fetal cortical slices. Cells used for calculation were in anaphase or telophase and displayed the following characteristics: oRG cells: pVim⁺, pH3⁺ cells in the iSVZ or oSVZ that displayed a basal fiber but no apical ventricular contact; IP cells: Tbr2⁺ cells in the iSVZ or oSVZ that were pVim⁺ and displayed no basal or apical fiber.

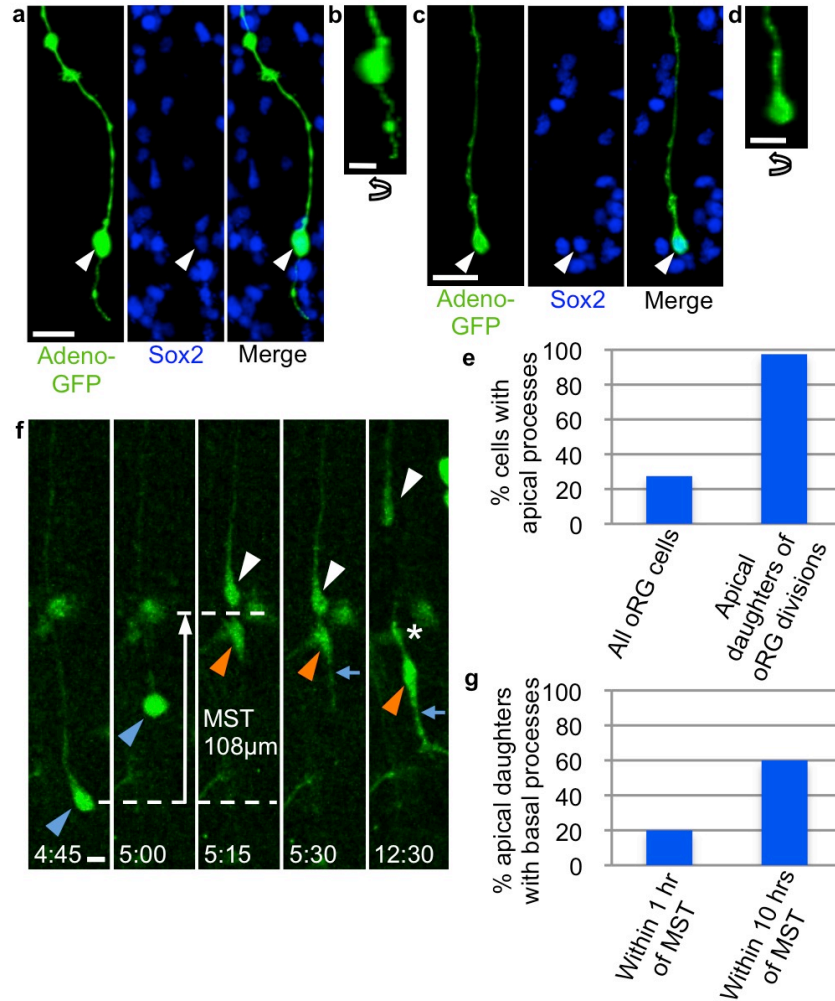


Figure 3. Apical and basal processes on oRG cells and oRG apical daughters. **a)** oRG cell with apical process in GW18 human fetal oSVZ, identified by morphology after 18-hour Adeno-GFP infection followed by fixation and Sox2 staining. Scale bar, 20 μm. **b)** Z-plane analysis of cell in (a) rotated 90° confirms presence of apical process. Scale bar, 10μm. **c)** oRG cell lacking apical process in GW18 human fetal oSVZ, identified by morphology after Adeno-GFP infection and by Sox2 positivity. Scale bar, 20μm. **d)** Z-plane analysis of cell in (c) rotated 90° confirms lack of apical process. Scale bar, 10μm. **e)** Quantification of presence of apical process on all oRG cells in the GW16/18 human fetal i/oSVZ, and on apical daughters of oRG cell divisions after time-lapse imaging of GW16/18 human fetal cortex. All apical processes on apical daughters were produced within 1 hour of MST. **f)** Time-lapse stills of a dividing oRG cell (blue arrowhead) in GW18 human fetal cortical slice labeled with Adeno-GFP. The

oRG cell undergoes MST and produces an apical daughter (orange arrowhead) and a basal daughter (white arrowhead). The basal daughter retains the basal fiber and becomes a self-renewed oRG cell. The apical daughter produces an apical process immediately after MST (blue arrow), and a basal process several hours after MST (asterisk), adopting bipolar morphology. Scale bar 10 μ m. **g)** Quantification of presence of basal process on apical daughters of oRG cell divisions after time-lapse imaging in GW16/18 human fetal cortex. Unlike the apical process, the basal process often takes more than 1 hour to begin growing after MST.

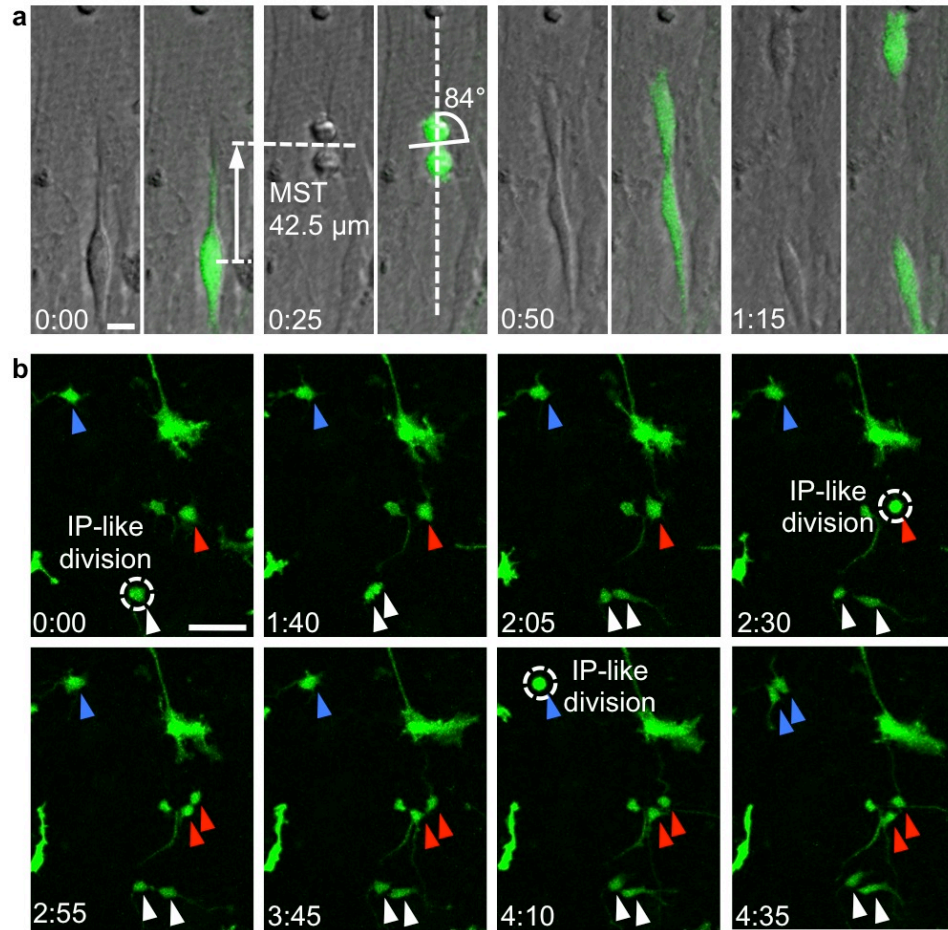


Figure 4. Dissociated cortical progenitor cells display MST and horizontal spindle orientation. a) oRG-like cell in dissociated culture undergoes MST followed by division with horizontal cleavage angle. Dissociated cortical cells were infected with low-titer GFP adenovirus or retrovirus and grown in culture for up to 5 weeks. Transmitted light microscopy allowed visualization of condensed chromatin for quantification of spindle orientation. Scale bar, 10 μ m. **b)** Multiple IP-like cell divisions in culture, which contrast with oRG-like divisions by their lack of MST. Individual multipolar cells were followed (blue, red, and white arrowheads), and over a period of less than 5 hours, each cell underwent mitosis (dotted circle) without MST, producing two multipolar daughter cells. Scale bar, 50 μ m.

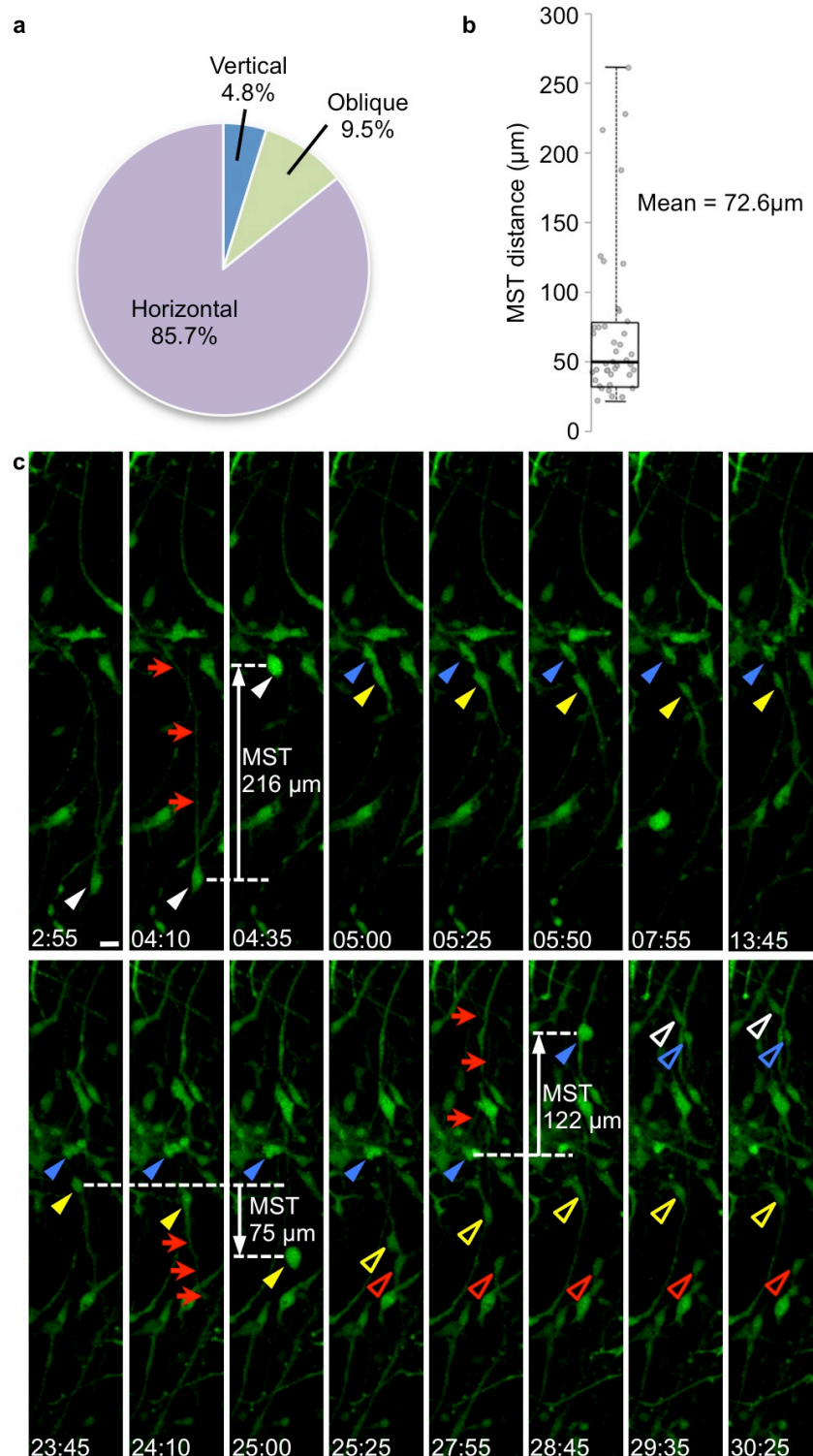


Figure 5. MST and establishment of a horizontal spindle orientation are cell-intrinsic processes. a) Quantification of cleavage angles in oRG-like cells in dissociated culture in which transmitted light microscopy allowed visualization of spindle orientation. **b)** Box plot of MST distances for oRG-like

divisions in dissociated culture. **c)** Time-lapse stills of dissociated, Adeno-GFP labeled GW16 human neocortical progenitor cell divisions. oRG-like cell (white arrowhead) with basal process (red arrows) undergoes MST along the basal process and divides at 4:35 to produce two daughter cells: a “basal” daughter (blue arrowhead) and an “apical” daughter (yellow arrowhead). The apical daughter grows a basal fiber (red arrows) in the opposite direction as the original basal fiber, and subsequently undergoes MST in the direction of the newly-generated fiber and divides at 25:00 to produce two daughter cells (open yellow arrowhead, open red arrowhead). The basal daughter of the first division extends its basal fiber (red arrows) in the same orientation as the original basal fiber, and undergoes MST in the direction of this fiber. This cell divides at 28:45 to produce two daughter cells (open white arrowhead, open blue arrowhead). Scale bar, 20 μm .

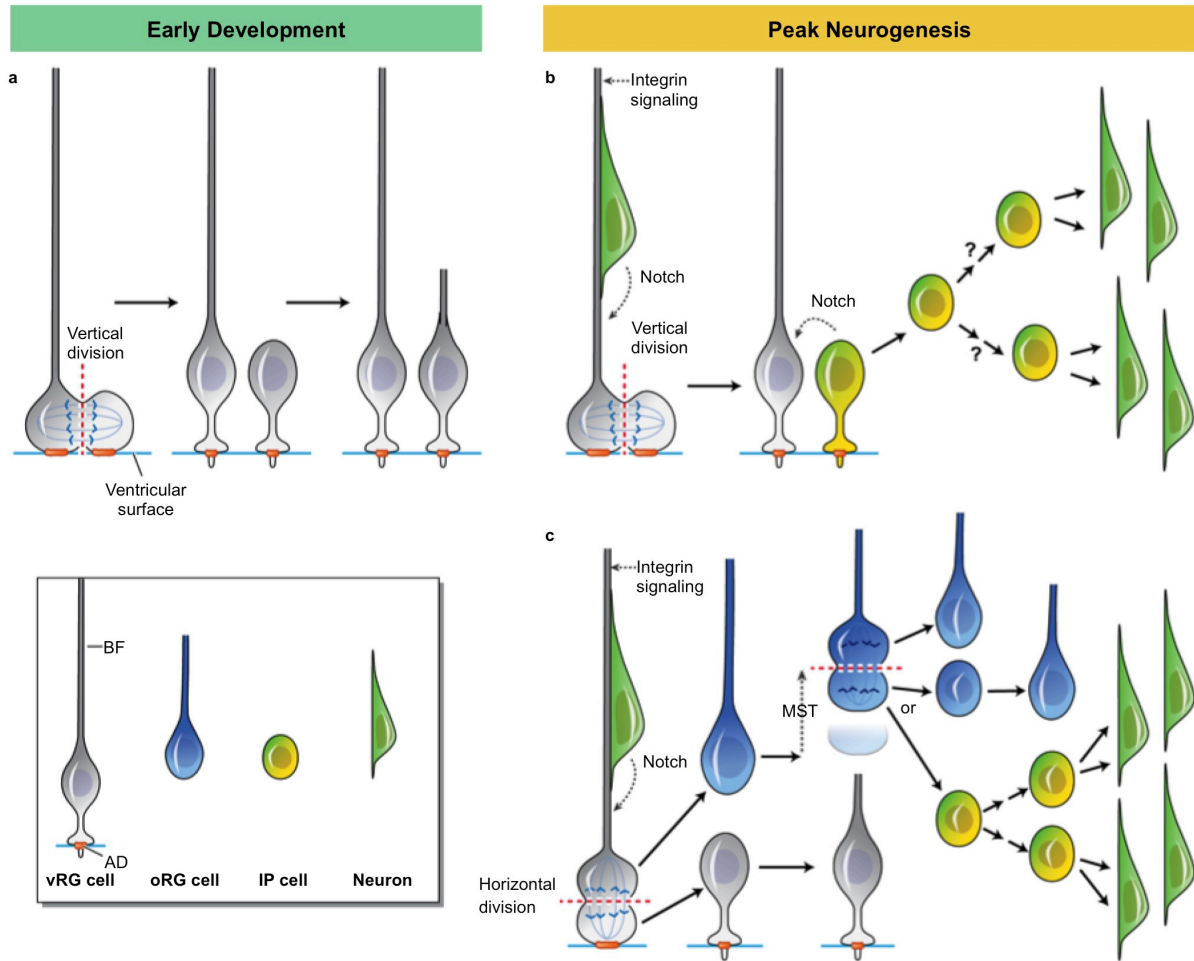
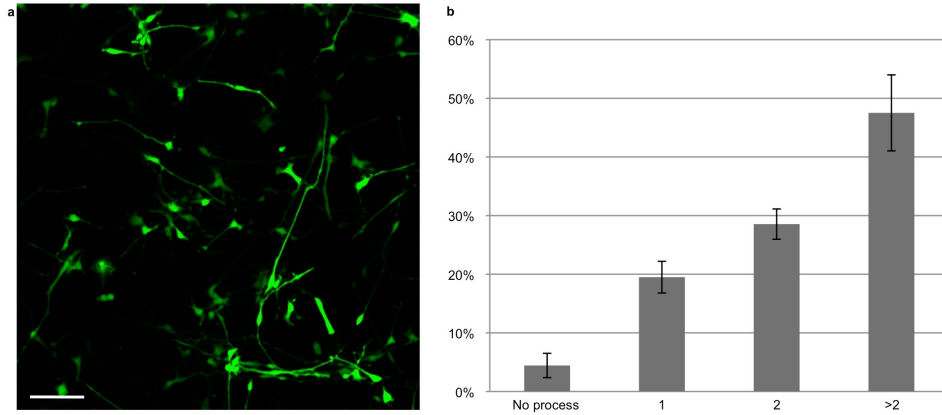


Figure 6. Model of cleavage angle regulation of cell fate during human cortical development. a) During early development, vRG divisions at the VZ are likely vertical, resulting in one daughter inheriting the basal fiber, and both daughters inheriting half of the apical domain (AD), orange. The daughter that retains the basal fiber maintains its apical contact and becomes a self-renewed vRG cell, while the daughter that does not receive the basal fiber likely also maintains its apical contact, generates a new basal fiber, and adopts a vRG cell identity, thereby increasing the vRG progenitor population. **b)** During peak neurogenesis, vRG divisions can either be vertical or horizontal/oblique. vRG division with vertical cleavage plane results in both daughter cells inheriting half of the AD. The cell that retains the basal fiber receives Notch and Integrin signaling via the basal fiber, maintains its apical contact and becomes a self-renewed vRG cell. The cell that does not inherit the basal fiber begins to express IP cell

markers, including Notch ligands, thereby contributing to Notch activation of neighboring vRG cells. The newly-generated IP cell delaminates from the apical adhesion belt during the next cell cycle and migrates in a basal direction, where it may undergo multiple rounds of neurogenic divisions. **c)** vRG division with a horizontal (or oblique) cleavage plane results in the more apical daughter inheriting the entire AD, regrowing a basal fiber, and becoming a self-renewed vRG cell. The more basal daughter inherits the basal fiber, rapidly exits the VZ, and adopts an oRG cell fate. The newly-generated oRG cell continues to divide horizontally, with the basal daughter inheriting the basal fiber and maintaining oRG cell identity. The apical daughter of horizontal oRG cell divisions either regrows a new fiber and adopts oRG cell fate, expanding the oRG cell population, or becomes an IP cell and undergoes multiple rounds of neurogenic divisions.



Supplementary Figure S1. Composition of primary dissociated cortical progenitor cultures. a) Representative image of dissociated culture from GW16 human fetal cortex infected with Adeno-GFP. Scale bar, 100 μm . **b)** Quantification of percentage of cells displaying each morphology type based on process number. Error bars represent standard deviation of percentile count from four random fields of approximately 770x770 μm .

Supplementary Movie S1. vRG cells dividing at ventricular surface. Human vRG cells in GW16 cortical slice labeled with Adeno-GFP displaying INM and undergoing a mixture of horizontal and vertical divisions.

This movie can be accessed online at:

<http://www.nature.com/ncomms/journal/v4/n4/full/ncomms2647.html>

Supplementary Movie S2. Horizontal vRG divisions produce oRG cells. A vRG cell in GW16 human fetal cortical slice undergoing INM and dividing with a horizontal cleavage angle, producing a basal daughter with oRG morphology, and an apical daughter with vRG morphology.

This movie can be accessed online at:

<http://www.nature.com/ncomms/journal/v4/n4/full/ncomms2647.html>

Supplementary Movie S3. oRG cells divide horizontally to self-renew. An oRG cell in GW18 human fetal cortical slice undergoing MST with horizontal cleavage plane orientation.

This movie can be accessed online at:

<http://www.nature.com/ncomms/journal/v4/n4/full/ncomms2647.html>

Supplementary Movie S4. INM-like behavior in dissociated cells. A bipolar cell in dissociated cortical progenitor cell culture displaying oscillatory behavior, but not definitive INM. This behaviour contrasts with MST, displayed by an oRG-like cell at the end of the movie.

This movie can be accessed online at:

<http://www.nature.com/ncomms/journal/v4/n4/full/ncomms2647.html>

Supplementary Movie S5. Symmetrical oRG cell division. An oRG-like cell in dissociated cortical progenitor cell culture undergoing MST and dividing to produce two oRG-like daughters, which also undergo MST and divide.

This movie can be accessed online at:

<http://www.nature.com/ncomms/journal/v4/n4/full/ncomms2647.html>

METHODS

Fetal tissue collection

Donated fetal brain tissue was collected from elective pregnancy termination specimens at San Francisco General Hospital, usually within 2 h of the procedure. Gestational age was determined using fetal foot length. Brain tissue was transported in L-15 medium on ice to the laboratory for further processing. Tissues were collected only with previous patient consent and in strict observance of legal and institutional ethical regulations. Research protocols were approved by the Gamete, Embryo, and Stem Cell Research Committee (institutional review board) at University of California, San Francisco.

Immunohistochemistry, imaging and cleavage angle analysis

Brain tissue was fixed in 4% PFA in PBS at 4 °C for 3 days, dehydrated in 30% sucrose in PBS, embedded and frozen at -80 °C in O.C.T. compound (Tissue-Tek), sectioned on a Leica CM3050S (50 or 20 µm) and stored at -80 °C. Cryosections were subjected to heat/citrate-based antigen retrieval for 10 min and permeabilized and blocked for 3-4 hours in PBS plus 0.1% Triton X-100, 10% serum, 0.2% gelatin. Primary incubations were performed at 4 °C overnight. Washes and secondary incubations were standard procedures. Images were acquired on a Leica TCS SP5 broadband laser confocal microscope. Composite images were automatically stitched upon acquisition using ‘Tilscan’ mode of Leica software. Images with morphological information are maximum intensity projections collected with at least 1-µm z-step size. Mitotic spindle orientations of cells in anaphase or telophase were measured using Screen Protractor (Iconico). The cleavage plane angle was calculated by determining the angle between the equatorial plate and the ventricular surface (vRG cells), the basal fiber (oRG cells), or the nearest basal fiber (IP cells). For quantification, vRG cells were defined as pVim⁺ cells at the ventricular surface with a basal fiber, oRG cells were defined as pVim⁺ cells in the iSVZ or oSVZ with a basal fiber but no apical ventricular contact (end foot), and IP cells were defined as pVim⁺ cells in the iSVZ or oSVZ that were Tbr2⁺ and

displayed no basal or apical process. All proportions were calculated from between 35-60 cells in at least 5 different sections for each age generated from at least 2 different tissue samples for each age.

Primary antibodies were: goat anti-SOX2 (Santa Cruz sc-17320, 1:250), rabbit anti-TBR2 (Millipore AB9618 or Abcam ab23345, 1:400), mouse anti-phospho-vimentin (MBL International D076-3S (Ser 55), 1:500), chicken anti-GFP (Aves Labs GFP-1020, 1:1,000), rabbit anti-phospho-histone-H3 (Abcam ab1791, 1:500), rabbit anti-nestin (Abcam ab5968, 1:200) and rabbit anti-PAX6 (Covance PRB-278P, 1:200). Secondary antibodies were: AlexaFluor 488 (1:1,000), 546 (1:500), 568 (1:500), 594 (1:500), or 647 (1:500)-conjugated donkey anti-goat, -rabbit or -mouse IgG, or goat anti-chicken IgY (Invitrogen).

Viral infection, slice culture and real-time imaging

For time-lapse imaging experiments, brain tissue was transferred to ice-chilled artificial cerebrospinal fluid (ACSF; 125 mM NaCl, 2.5 mM KCl, 1 mM MgCl₂, 2 mM CaCl₂, 1.25 mM NaH₂PO₄, 25 mM NaHCO₃, 25 mM d-(+)-glucose, bubbled with 95% O₂/5% CO₂), and blocks of cortical tissue were trimmed and imbedded in 4% low melting point agarose in ACSF. 250–300- μ m vibratome slices were generated and transferred to and suspended on Millicell-CM slice culture inserts (Millipore) in cortical slice culture medium, containing 66% BME, 25% Hanks, 5% FBS, 1% N-2, 1% penicillin, streptomycin and glutamine (all Invitrogen) and 0.66% d-(+)-glucose (Sigma). CMV-GFP adenovirus (Vector Biolabs, 1 x 10⁶ c.f.u.) was directly applied to slices, and slices were cultured at 37 °C, 5% CO₂, 8% O₂ for ~24 h, as described previously (Hansen 2010). Cultures were then transferred to an inverted Leica TCS SP5 with an on-stage incubator (while streaming 5% CO₂, 5% O₂, balanced N₂ into the chamber), and imaged using a x10 or x40 air objective at 15–25-min intervals for up to 6 days with intermittent repositioning of the focal planes. Maximum intensity projections of the collected stacks (~30 μ m at ~2.5- μ m step size) were compiled and generated into movies, which were analyzed using Imaris. Cleavage angle analysis was performed in a similar manner as for fixed tissue, using only divisions in which the cleavage furrow from anaphase through telophase was clearly visible. Quantification of vRG divisions in slices was performed

on two or more slices each from n=5 individual tissue samples aged GW16-18. A total of 70 vRG cell divisions were analyzed. Daughter cell morphology could not be definitively determined in all cases because imaging sessions could only last approximately 24 hours due to subsequent distortion of the ventricular surface *in vitro*, and because in some cases, cells moved outside of the field of imaging. Due to these issues, analysis of daughter cell fate after vRG division was performed on 31 pairs of daughter cells out of the 70 total pairs of daughter cells.

Dissociated cortical progenitor culture and real-time imaging

GW14-16 cortex was separated from meninges and cut into small pieces using a razor blade. Cells were dissociated by incubation with papain (Worthington Biochemical Corporation) at 37 °C for 20 min followed by addition of DNase I and trituration. Dissociated cells were plated at a density of 250,000 cells per well in 12-well cell culture plates (Greiner Bio-one) pre-coated with matrigel (BD Biosciences). Cultures were maintained in a DMEM-based dissociated culture medium containing 1% N-2, 1% B-27 supplement, 1% penicillin, streptomycin and glutamine (all Invitrogen), sodium pyruvate (0.11mg/mL), 1mM N-acetyl-cysteine, with or without 10ng/mL hFGF. CMV-GFP adenovirus (Vector Biolabs, 1×10^6 c.f.u.) or replication-incompetent enhanced-GFP-expressing retrovirus (1×10^6 colony forming units (c.f.u.) were applied to cells, which were cultured at 37 °C, 5% CO₂, 8% O₂ until cells began expressing GFP (~24-48 h). Cultures were then transferred to an inverted Leica TCS SP5 with an on-stage incubator (while streaming 5% CO₂, 5% O₂, balance N₂ into the chamber), and imaged in both the GFP and transmitted light channels using a x10 objective at 35-min intervals for up to 10 days. Movies were analyzed using Imaris. Cleavage angle analysis was performed in a similar manner as for fixed tissue, using only divisions in which the condensed chromatin in anaphase or telophase was visible by transmitted light. A total of 41 oRG-like divisions from n=2 dissociated tissue samples were analyzed.

To determine the proportions of cell morphologies within dissociated cultures, cells were labeled as described above, and all cells that were bright enough to discern morphology were counted in four

random fields of approximately 770x770 μm . For each cell, process number was defined as one of four groups: 0 (no discernable process), 1, 2, or >2 (multipolar). The average of the four proportion calculations from each field was then calculated for each group.

Quantification of apical and basal processes

To determine the proportion of oRG cells that display apical processes, GW16-18 human fetal cortical slices were infected with Adeno-GFP, cultured as described above for 18 hours, fixed, and stained for GFP, Sox2 and nestin. Confocal imaging was performed using a x63 objective and images were analyzed using Imaris. A total of 51 cells were analyzed, and only cells that displayed a basal fiber and were GFP+/Sox2+ were used for quantification of apical process presence and length. Additionally, all oRG cells used for quantification were determined to be nestin+. For analysis of apical and basal processes in apical daughters of oRG division, time-lapse imaging of GW16-18 slices was performed as described above on at least two slices each from n=3 individual tissue samples, and movies were analyzed using Imaris. 40 oRG cell divisions in total were analyzed, with oRG cells defined based on oRG morphology (presence of a basal fiber, lack of ventricular contact) and mode of division (MST). After MST, An apical daughter was determined to have an apical process if a ventricular-directed process of any length appeared in the next cell cycle. An apical daughter was determined to have a basal process if a pial-directed process of any length appeared in the next cell cycle.

Statistics

For all measurements of cleavage angle proportions in fixed cryosections, between 35-60 cells were analyzed from at least 5 sections for each age and cell type quantified. Proportions were compared pairwise using a Pearson's Chi Square test.

CHAPTER 3

Control of outer radial glial cell mitosis and progenitor zone expansion in the human brain

This chapter is a work in progress by:

LaMonica, B.E., Lui, J.H., Gertz, C.C., and Kriegstein, A.R.

SUMMARY

Evolutionary expansion of the neocortex underlies the unique cognitive abilities of humans, and is partially attributed to a relative abundance of neural stem cells in the fetal brain called outer radial glia (oRG). oRG cells display a characteristic division mode, mitotic somal translocation (MST), in which the soma rapidly translocates towards the cortical plate immediately prior to cytokinesis. The molecular motors driving MST are unknown, hindering exploration of its function in human brain development and disease. Here, we show that MST requires activation of the Rho effector ROCK and non-muscle myosin II-dependent actomyosin contraction. MST is independent of mitosis, and does not require microtubule polymerization or centrosomal guidance. We further find that inhibition of MST in human slices decreases progenitor zone expansion and delivery of committed neural precursors closer to the cortical plate. We propose that defects in MST may partially underlie cortical malformations currently attributed to disrupted neuronal migration.

INTRODUCTION

The human neocortex is characterized by a marked increase in size and neuronal number as compared to other mammals. Neural stem cells called outer radial glia (oRG), present in large numbers during human but not rodent brain development, are thought to underlie this expansion (Hansen 2010; Lui 2011). oRG cells are derived from ventricular radial glia (vRG), the primary neural stem cells present in all mammals (Malatesta 2000; Miyata 2001; Noctor 2001; Shitamukai 2011; Wang 2011; LaMonica 2013). Both progenitor cell types display basal processes oriented towards the cortical plate, along which newborn neurons migrate (Rakic 1971; Rakic 1972; Misson 1991; Hansen 2010). However, oRG cells reside primarily within the outer subventricular zone (oSVZ), closer to the cortical plate than vRG cells, and lack the apical ventricular contact characteristic of vRG cells (Chenn 1998; Hansen 2010). While vRG cell behavior, mitosis, and lineage have been extensively studied, much less is known about regulation of oRG cell proliferation and the unique mitotic behavior of these cells (Qian 1998; Bentivoglio 1999; Hartfuss 2001; Noctor 2001; Noctor 2004; Noctor 2008; Taverna 2010). During a process called mitotic somal translocation (MST) that occurs immediately prior to cytokinesis, the oRG soma rapidly translocates a distance of several cell diameters along the basal fiber towards the cortical plate (Hansen 2010). Due to the relative abundance of oRG cells in humans, it has been hypothesized that genetic mutations causing significant brain malformations in humans, but minimal phenotypes in mouse models, may affect oRG cell-specific behaviors such as MST (Lamonica 2012). However, the molecular motors driving MST have not been identified, hindering exploration of the function of MST in human brain development and its possible role in disease.

RESULTS

oRG cell MST requires myosin II but not microtubule motors

MST is reminiscent of interkinetic nuclear migration of neuroepithelial and vRG cells, in which nuclei of cycling cells migrate back and forth along the basal fiber between the apical and basal boundaries of the ventricular zone (VZ). Interkinetic nuclear migration is controlled by the centrosome, the microtubule motors kinesin and dynein, and associated proteins, with actomyosin motors playing an accessory role (Taverna 2010). As oRG cells are derived from vRG cells and display analogous nuclear movements, we initially hypothesized that MST requires similar molecular motors as interkinetic nuclear migration. To determine the relative contributions of microtubule motors and actomyosin to MST, we applied inhibitors of microtubule polymerization and non-muscle myosin II (NMII, the most well-characterized myosin in brain development (Tullio 2001; Vallee 2009)) to human fetal cortical slice cultures. We performed time-lapse imaging of oRG cell behaviors, and quantified translocation (MST) and division frequency in each slice before and after addition of inhibitors or DMSO (control) (Fig. 1A-E and S1). Surprisingly, treatment of slices with a low concentration (5 μ M) of blebbistatin, a selective NMII inhibitor, caused a significantly greater reduction in translocations than in divisions. Conversely, treatment with the microtubule depolymerizing reagent nocodazole (1 μ M) reduced divisions significantly more than translocations. Additionally, nocodazole, but not DMSO or blebbistatin, decreased the proportion of translocations that ended in division. We found that oRG cells express two isoforms of NMII: NMIIa and NMIIb (Fig. 1F, G and Fig. S2), which have both been shown to play essential roles in neuronal migration (Vicente-Manzanares 2009). Thus, MST and mitosis are mutually dissociable in oRG cells. MST requires NMII activation, but not microtubule polymerization, while mitosis requires microtubule polymerization, but not NMII activation.

To control for non-cell-autonomous effects and to enable examination of subcellular mechanisms, we used dissociated progenitor cell cultures. We previously observed that oRG-like cells undergo MST in dissociated fetal human cortical cultures (LaMonica 2013). To confirm oRG identity of oRG-like cells, we performed fate staining on daughter cells after MST division (Fig. 2A-C and S3). Similar to oRG cells in slice culture (Hansen 2010), daughters of MST divisions in dissociated culture expressed SOX2 (65 out of 65) and PAX6 (17 out of 17), usually expressed nestin (18 out of 24), rarely expressed TBR2 (2 out of 34), and never expressed β III-tubulin (0 out of 20). As in slice culture, we observed expression of both NMIIa (14 out of 14 cells) and NMIIb (10 out of 10 cells) in dissociated oRG cell daughters (Fig. 2I, J). We concluded based on morphology, behavior, and marker expression, that cells undergoing MST in dissociated culture are oRG cells, validating the use of dissociated cultures to study oRG cell behaviors. We then quantified translocation (MST) and division frequency after motor protein inhibition. Similar to results in slice culture, blebbistatin treatment reduced translocations significantly more than divisions, while nocodazole treatment reduced divisions without significantly affecting translocations (Fig. 2D-H). Upon nocodazole wash-out, cells that remained rounded up after MST underwent cytokinesis, suggesting that the effects of nocodazole were not due to cell death (Fig. S4). Furthermore, inhibitor-treated cultures did not display increased staining for cleaved caspase-3, confirming that the effects of inhibitor treatment were reversible and could not be attributed to apoptosis (Fig. S5). Thus, results in dissociated culture confirm observations in slice culture that MST and mitosis are mutually dissociable in oRG cells. Intact microtubules are required for oRG cell mitosis, but not for MST, while NMII is required for oRG cell MST, and is relatively less important for mitosis.

MST depends on intact microtubules but not centrosomal guidance

Though intact microtubules are not required for oRG cell MST in humans, nocodazole treatment significantly increased MST distance in both slice culture and dissociated cells (Fig. 3A). Based on previous observations in rodent (Wang 2011), we hypothesized that the centrosome migrates into the

basal fiber prior to translocation, remains connected to the nucleus via a microtubule cage, and ultimately determines the location of translocation cessation and cytokinesis. Nocodazole treatment would disrupt nucleus-centrosome coupling, eliminating the "stop" signal for translocation. To determine whether the centrosome precedes the nucleus into the basal process, we performed time-lapse imaging of centrosome behavior in dissociated human oRG cells after transfection with a construct encoding the centrosomal protein Centrin-2 fused to the fluorescent reporter dsred (Fig. S6) (Tanaka 2004). While centrosome location was variable during interphase, centrosomes consistently returned to the soma prior to MST and remained adjacent to the nucleus throughout translocation (Fig. 3B, D). In contrast, during saltatory migration of other cells in dissociated culture, the centrosome often preceded the nucleus into the leading process prior to a migratory step (Fig. 3C, D). Interestingly, somal translocation distances were much greater during MST than during saltatory migration steps, suggesting that an increased nuclear translocation distance may limit the role of the centrosome during MST (Fig. 3E). We concluded that translocation of the centrosome into the basal fiber prior to nuclear translocation is not required for MST. Instead, microtubule polymerization may directly regulate actomyosin contractility (Schaar 2005).

MST requires ROCK activation but not calcium influx

We hypothesized that NMII-mediated actin polymerization in oRG cells depends either on calcium influx or the Rho-ROCK pathway, both of which are upstream activators of NMII that regulate neuronal migration (Komuro 1992; Guan 2007; Govek 2011; Shinohara 2012). To test this hypothesis, we applied a panel of calcium channel inhibitors including the ryanodine receptor blocker ruthenium red (RR, 50 μ M), IP₃-gated calcium channel blocker 2-APB (50 μ M), L-type calcium channel blocker nifedipine (nifed, 1 μ M), and nonspecific calcium channel blocker NiCl₂ (50 μ M) as well as the ROCK inhibitor Y-27632 (ROCKi, 10 μ M), to dissociated human progenitor cultures and quantified translocation (MST) and division frequency (Fig. 4A). Surprisingly, calcium channel blockade did not specifically inhibit divisions or translocations, suggesting that calcium influx is not the initial trigger for MST. In contrast, ROCKi

mimicked the effects of blebbistatin treatment, greatly reducing translocations without significantly affecting divisions. Consistent with these results, inhibition of myosin light chain kinase (MLCK) with ML-7 (10 μ M), an activator of NMII that is downstream of Ca²⁺-calmodulin but not ROCK, had no effect on translocations or divisions (Fig. 4A). ROCK- and NMII-dependent actomyosin contraction may occur throughout the soma and basal process, as we often observed shortening and thinning of the primary process during MST in dissociated oRG cells (Fig. S7). This observation is consistent with NMII expression throughout oRG cell processes (Fig. 2I, J). Thus, both NMII and activated ROCK, but not calcium influx, are required for oRG cell MST.

MST promotes developmental oSVZ expansion and delivery of committed neural precursors closer to the cortical plate

We have demonstrated here that MST and mitosis can be uncoupled, suggesting that the function of MST is distinct from that of mitosis. MST moves neural stem cells away from the ventricle, which may reduce cell crowding and promote radial over tangential expansion of progenitor zones. MST could also accelerate fetal brain development by delivering oRG daughters, including IP cells and their neuronal progeny, closer to their destinations in the cortical plate (Hansen 2010; Wang 2011). Suggestive of a role for MST in radial oSVZ expansion, we found that translocation distance and frequency of MST were increased in humans as compared to mice and ferrets, which display a smaller oSVZ and neocortex (Fig. 4B, C, S8). Furthermore, MST trajectory was overwhelmingly towards the cortical plate in human slices (Fig. 4D). To test the hypothesis that MST accelerates cortical development by promoting delivery of oRG daughters closer to the cortical plate, we inhibited MST in human fetal dorsal cortical slices for six days with 5 μ M blebbistatin. At the start of treatment, slices were incubated with BrdU for 24 hours to determine the distribution of newly generated oRG and IP cells. The oSVZ underwent more extensive basal expansion in control (DMSO-treated) as compared to blebbistatin-treated slices (Fig. 4E, F). Newly generated (BrdU+) oRG (Sox2+) cells and IP (Tbr2+) cells accumulated closer to the ventricle in

blebbistatin-treated slices, while these cells were delivered closer to the cortical plate in DMSO-treated slices (Fig. 4G-K). However, blebbistatin treatment did not alter the ratio of Tbr2+ to Sox2+ cells in the oSVZ as compared to DMSO ($p=0.38$, unpaired Student's *t* test), suggesting that MST does not directly control cell fate. Thus, NMII-dependent oRG cell MST is required for normal human oSVZ expansion during development and accelerates the delivery of committed neural progenitors (IP cells) towards the cortical plate.

DISCUSSION

Several evolutionary forces could have led to the unique dependence of MST on actomyosin motors. Nuclear translocation distance may dictate molecular motor dependence. Interkinetic nuclear migration and saltatory migration involve relatively smaller nuclear translocation steps, limiting the distance between the centrosome and the nucleus. The larger translocation distances of MST could hinder maintenance of tension between the centrosome and a perinuclear microtubule cage, making a centrosome-based mechanism impractical. Actomyosin motors are also approximately ten-fold faster than microtubule motors, and may be better suited to drive the rapid, large-amplitude translocations of MST (Mansson 2012). Additionally, we observed chromosome condensation and establishment of a metaphase plate during MST using time-lapse transmitted light microscopy, suggesting that prophase and metaphase occur prior to the completion of MST (Fig. 3B). Microtubule depolymerization occurs during prometaphase, and may preclude dependence of MST on microtubule motors (Rusan 2002).

MST requires ROCK and NMII activation, but not Ca^{2+} influx or MLCK activation. It is likely that in oRG cells, RhoA-activated ROCK either directly phosphorylates NMII, inhibits myosin phosphatase, or both, leading to actomyosin contraction and MST (Fig. 4L). The expression and activity of known cell cycle regulators support this model: RhoA is activated in a cell cycle-dependent manner by CDK1, and RhoA has been demonstrated to participate in the G_2 to M transition (Heng 2010). Interestingly, several genetic mutations that target the RhoA-ROCK-myosin II pathway lead to neurodevelopmental diseases in humans (Fig. 4L and Table S1). These mutations underlie cortical malformations that have largely been attributed to defective neuronal migration, but our results suggest MST may also be affected. Indeed, the expression patterns within the fetal human cortex of several cortical malformation candidate genes resemble the expression patterns of known radial glial genes, and hence of oRG cells, more closely than those of immature neuronal genes (Fig. S9). oRG cells comprise only a small proportion of neural

progenitor cells in mice as compared to humans (Wang 2011), and this difference could help explain why mouse models of cortical malformations such as microcephaly, periventricular heterotopia, and lissencephaly often display relatively mild phenotypes (Table S1). Future studies may reveal that mutations that affect the Rho-ROCK-NMII pathway and have minimal or altered phenotypes when reproduced in mouse models primarily target MST and not neuronal migration in human patients.

ACKNOWLEDGMENTS

We thank A. Alvarez-Buylla, J. Chan, and members of the Kriegstein laboratory for thoughtful discussions and critical reading of the manuscript. We thank W. Walantus, Y.Y. Wang and S. Wang for technical support. We thank Dr. J. Gleeson for use of the dsred-Cent2 plasmid. We thank the staff at the San Francisco General Hospital for providing access to donated fetal tissue. The research was made possible by a grant from the California Institute for Regenerative Medicine (Grant Number TG2-01153). Additionally, this work was supported by Bernard Osher and by award number R01NS075998 from the NINDS. The contents of this publication are solely the responsibility of the authors and do not necessarily represent the official views of CIRM or any other agency of the State of California, or of the NINDS or the NIH.

AUTHOR CONTRIBUTIONS

B.E.L. and A.R.K. designed the experiments; B.E.L. and J.H.L. carried out all experiments except those with ferret tissue and performed quantifications and analyses; C.C.G. performed ferret experiments; B.E.L. and A.R.K. wrote the initial manuscript; all authors edited and approved the final manuscript.

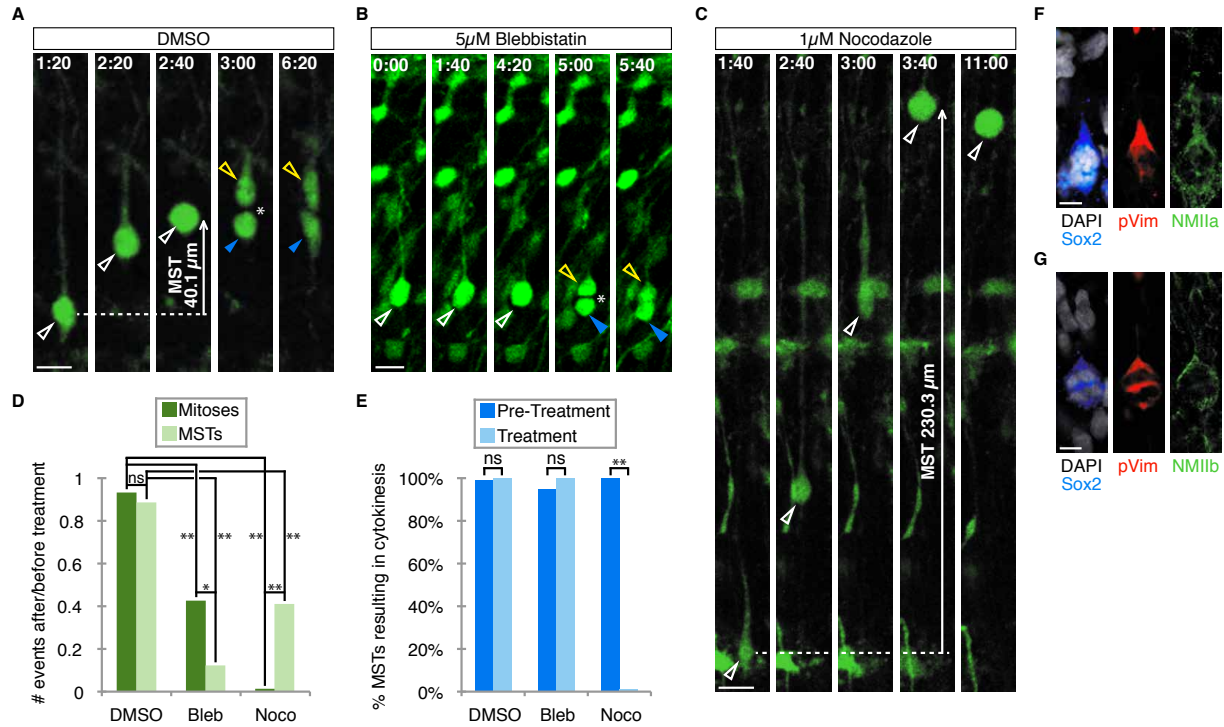


Figure 1. oRG cell MST requires myosin II but not microtubule motors. (A-C). Time-lapse stills of oRG cell behaviors in GW20.5 human fetal cortical slices labeled with Adeno-GFP. Time is in hours:minutes. Scalebars, 15 μ m. (A) In DMSO (control)-treated slice, the oRG cell (open white arrowhead) undergoes MST and cytokinesis (asterisk) to produce an apical daughter (closed blue arrowhead) and a basal daughter that retains oRG cell morphology (open yellow arrowhead). (B). In slice treated with the myosin II inhibitor blebbistatin, the oRG cell (open white arrowhead) divides (asterisk) without MST to produce an apical daughter (closed blue arrowhead) and a basal daughter that retains oRG cell morphology (open yellow arrowhead). (C). In slice treated with the microtubule depolymerizing agent nocodazole, the oRG cell (open white arrowhead) undergoes MST, fails to divide, and remains rounded up at the end of imaging. (D) Quantification of ratio of divisions and translocations (MSTs) after/before treatment for control (DMSO, 0.5%), blebbistatin (Bleb, 5 μ M), and nocodazole (Noco, 1 μ M). * p <0.01, ** p <0.0001, Fisher exact test. (E) Quantification of % MSTs resulting in cytokinesis. ** p <0.0001, Fisher exact test. (F-G) oRG cells in GW17.5 human fetal oSVZ express Sox2, the mitotic marker phospho-vimentin (pVim), NMIa, F, and NMIb, G. Scalebars, 5 μ m.

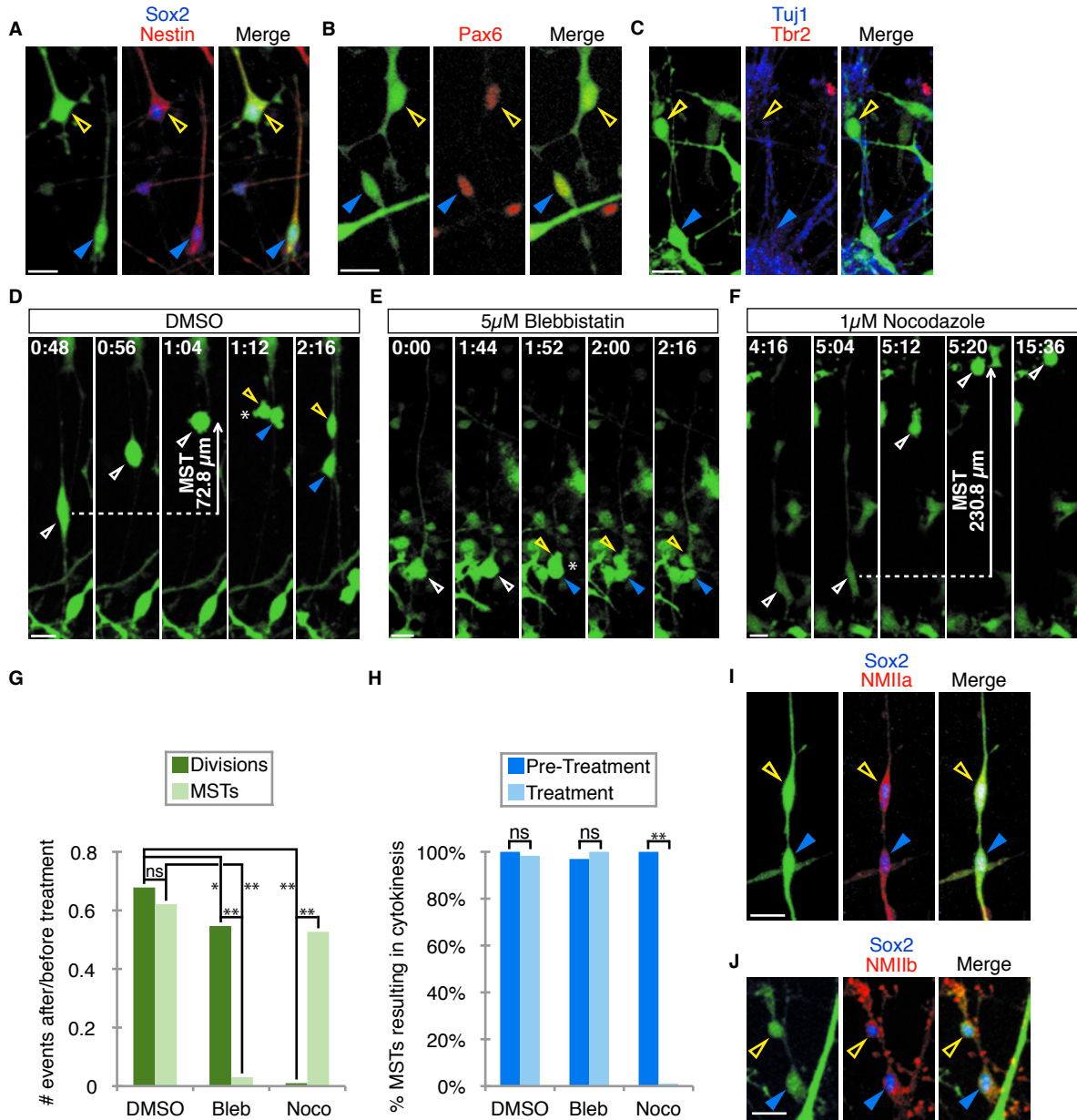


Figure 2. Dissociated human cortical progenitor cells express oRG cell markers and require myosin II for MST. (A-C) Fate staining of daughters (open yellow and solid blue arrowheads) of MST divisions in GW16.5 dissociated fetal human cortical progenitor cell cultures. Scalebars, 20 μ m. (A) Both cells express Sox2 and nestin. (B) Both cells express Pax6. (C) Neither cell expresses Tuj1 or Tbr2. (D-F). Time-lapse stills of oRG cells (open white arrowheads) in GW15.5-18.5 dissociated cultures labeled with Adeno-GFP. Time is in hours:minutes. Scalebars, 20 μ m. (D) oRG cell in DMSO (control)-treated culture undergoes MST and divides (asterisk) to produce an "apical" daughter (closed blue arrowhead) and a

"basal" daughter that retains oRG cell morphology (open yellow arrowhead). (E). Cell with oRG morphology in blebbistatin-treated culture divides (asterisk) without MST to produce an "apical" daughter (closed blue arrowhead) and a "basal" daughter that retains oRG cell morphology (open yellow arrowhead). (F) oRG cell in nocodazole-treated culture undergoes MST, fails to divide, and remains rounded up at the end of imaging. (G) Quantification of ratio of divisions and translocations (MSTs) after/before treatment for control (DMSO, 0.5%), blebbistatin (Bleb, 5 μ M), and nocodazole (Noco, 1 μ M). * p <0.05, ** p <0.0001, Pearson's chi-squared test or Fisher exact test (depending on sample size). (H) Quantification of % MSTs resulting in cytokinesis. ** p <0.0001, Fisher exact test. (I-J) Fate staining of daughters of MST divisions in GW16 dissociated fetal human cortical progenitor cell cultures. Daughter cells (indicated with open yellow and closed blue arrowheads) express the oRG cell marker Sox2 and the myosin isoforms NMIIa, I, and NMIIb. J. Scalebars, 20 μ m.

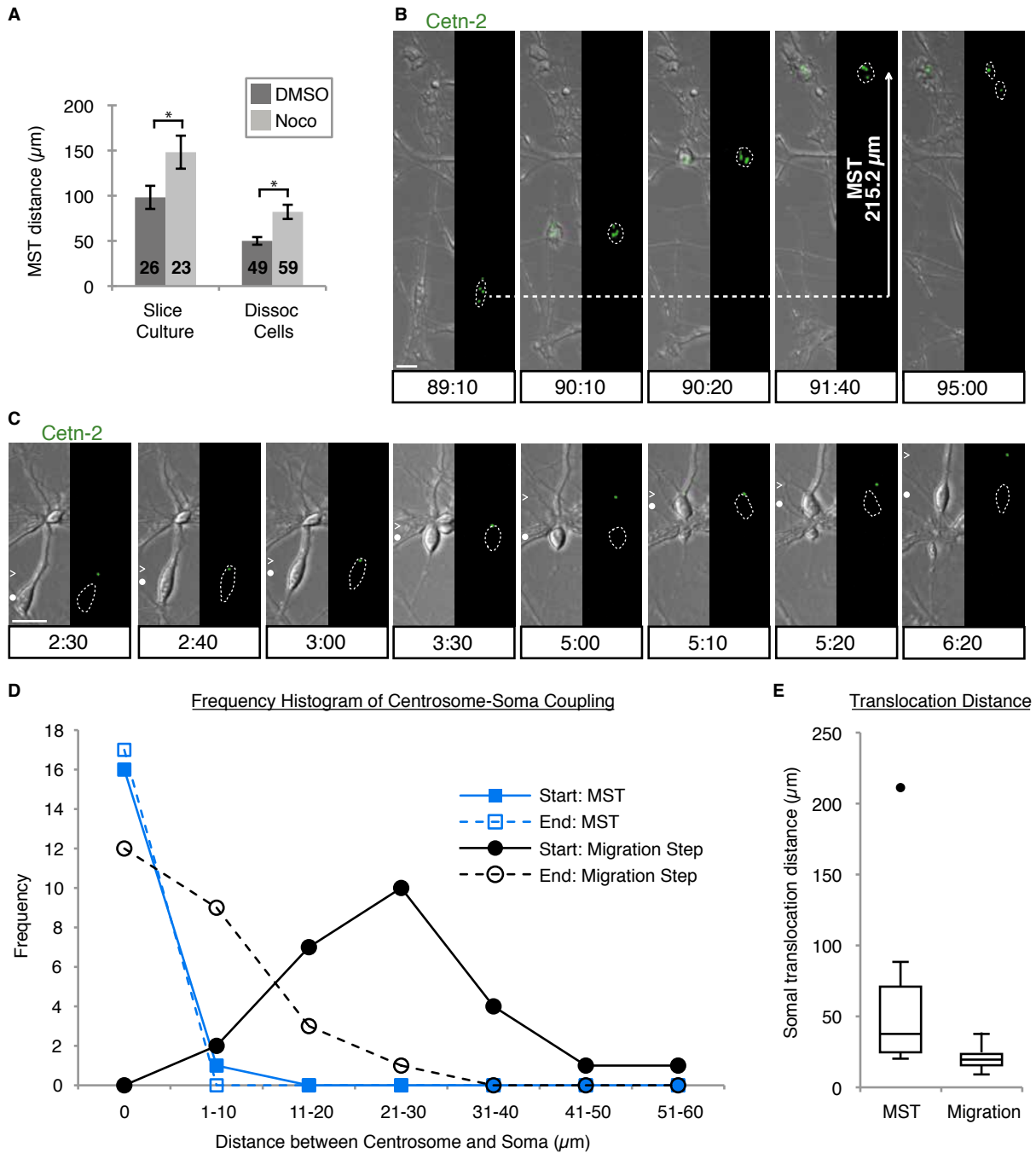


Figure 3. Role of microtubules and the centrosome in MST. (A) Quantification of MST distances after treatment with DMSO (control, 0.5%) or nocodazole (Noco, 1 µM). * $p < 0.05$, unpaired Student's t test. Error bars are SEM; sample size is indicated on each bar. (B-C) Time-lapse stills of oRG cell and centrosome behaviors in GW18.5 dissociated culture transfected with dsred-Cent2 to label centrosomes. Cent2 is false-colored in green. Each time point shows transmitted light and cent2 merge on the left, and

cent2 on the right, with a dashed white line depicting the outline of the soma. Time is in hours:minutes. Scalebars, 20 μ m. (B) oRG cell undergoes MST with centrosomes adjacent to the nucleus. (C) Centrosome behavior in cell undergoing saltatory migration. The location of the centrosome (white arrowhead) and the center of the soma (white circle) in the axis parallel to the direction of migration are shown on the left side of the transmitted light images. (D) Frequency histogram showing distances between the edge of the soma and the center of the centrosome furthest from the soma (C-S distance). The average CS-distance is 0.37 μ m at the start, and 0 μ m (centrosomes within the soma) at the end of MST, whereas the C-S distance during a migratory step averages 23.8 μ m at the start, and 4.2 μ m at the end. (E) Box plots depicting somal translocation distances of cells analyzed in D during MST (left) and migratory steps (right); n=17 for MSTs, n=21 for migratory steps.

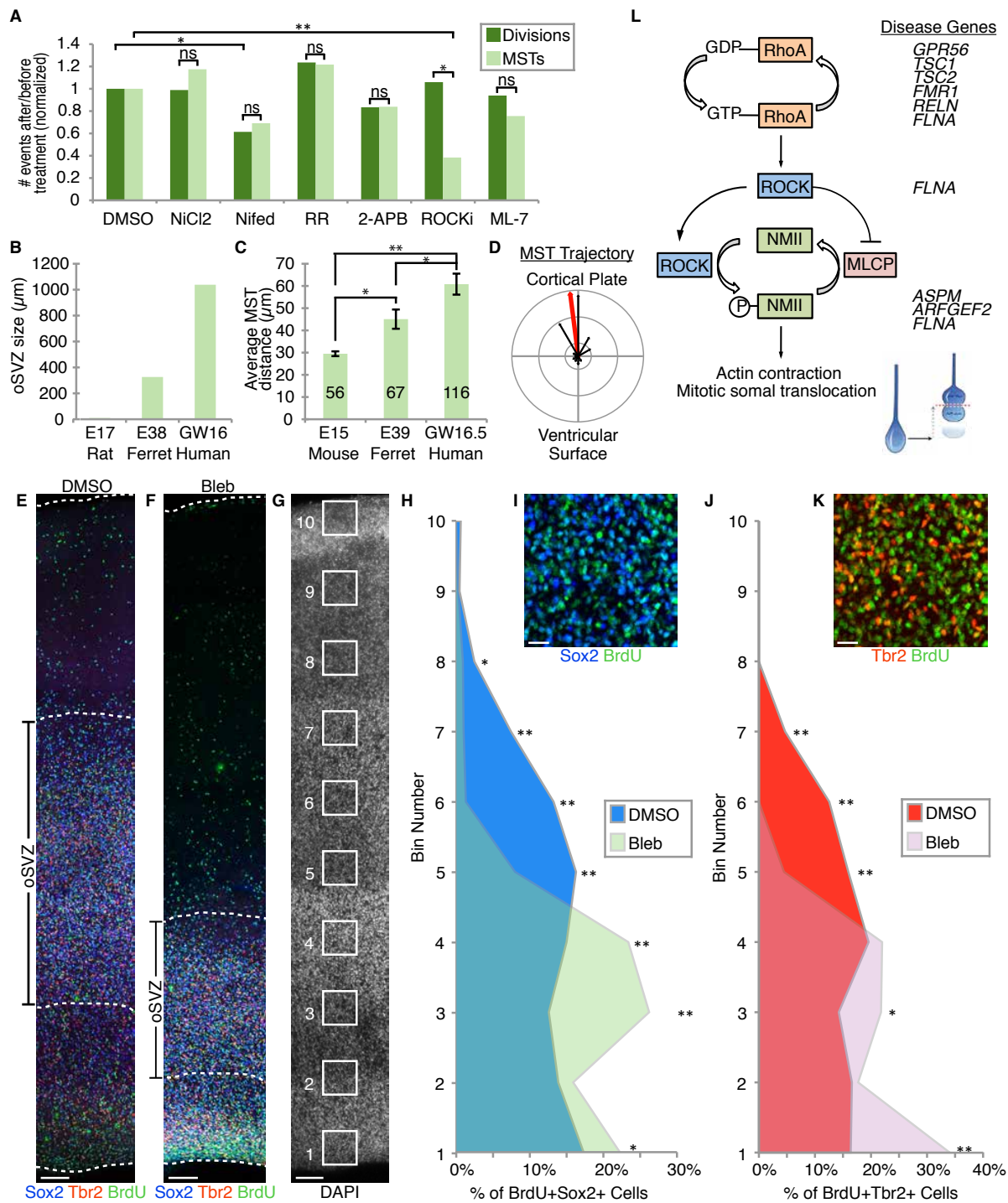
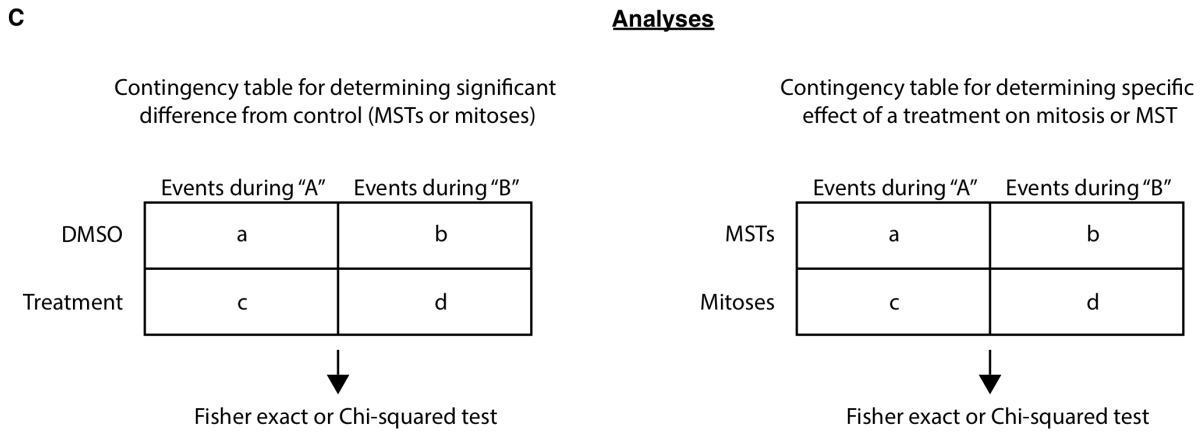
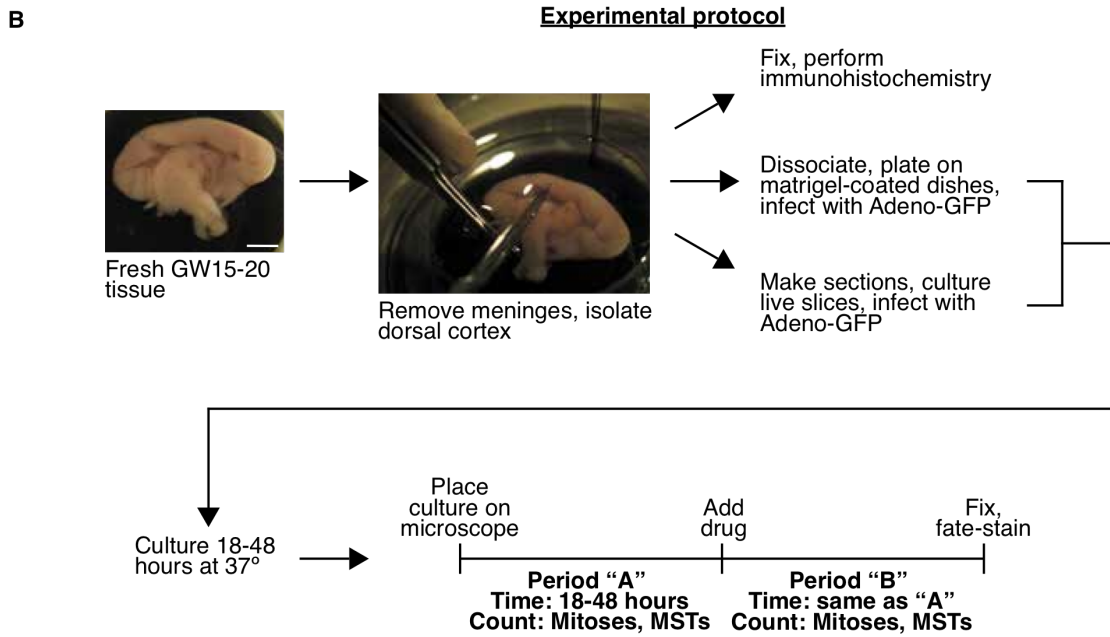
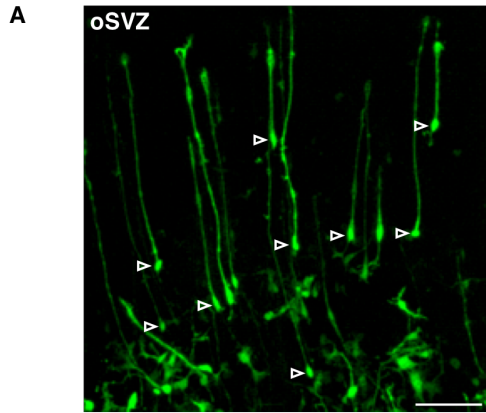
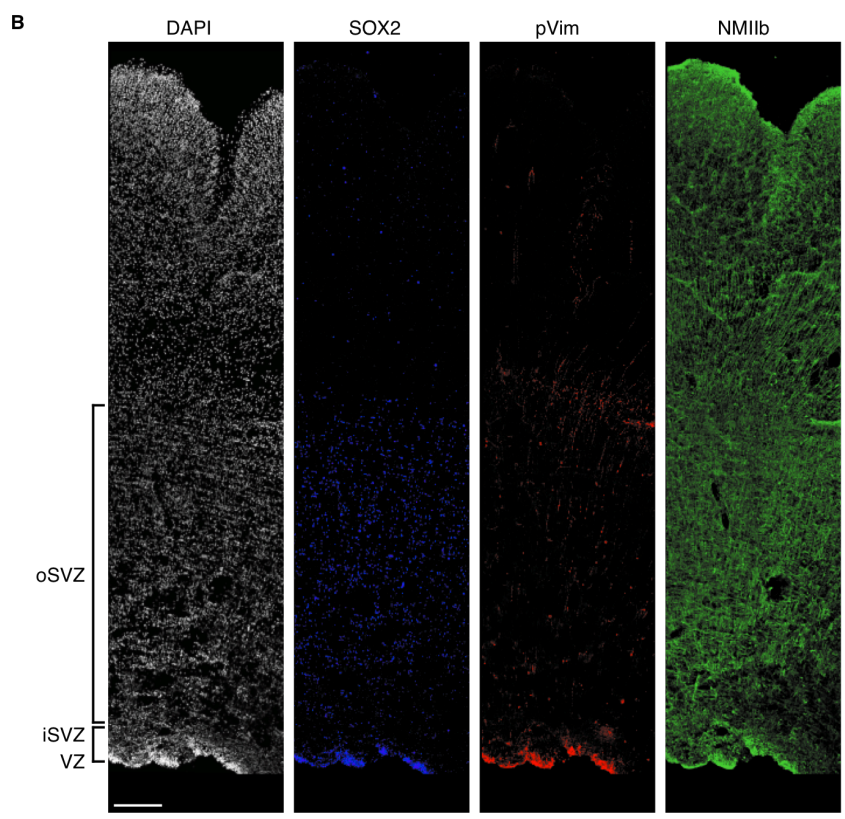
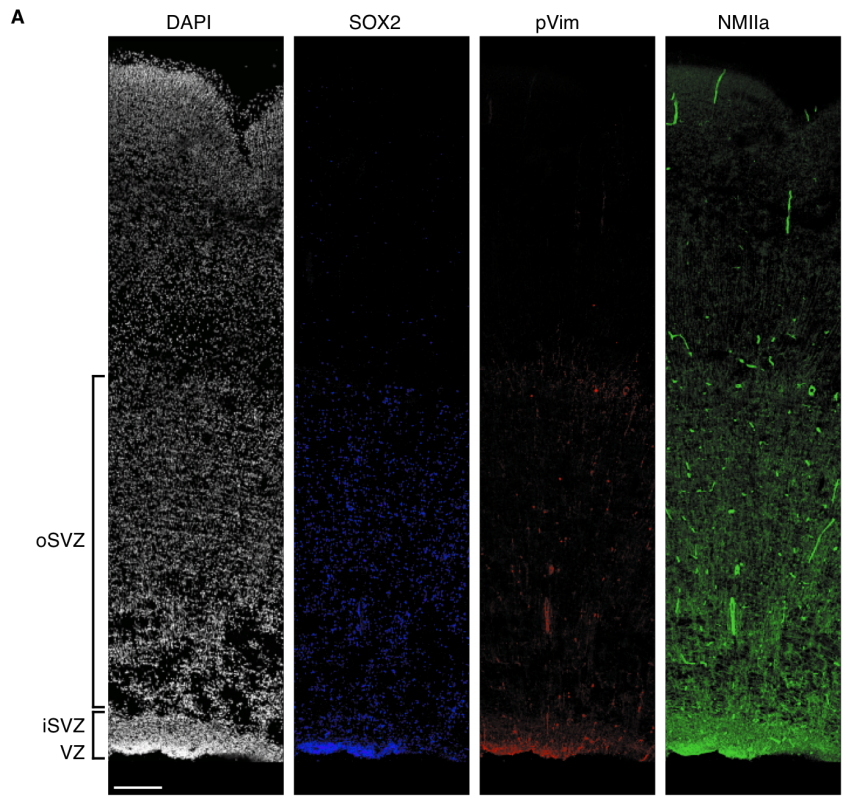


Figure 4. MST promotes developmental oSVZ expansion and delivery of committed neural precursors closer to the cortical plate. (A) Quantification of ratio of divisions and translocations (MSTs) after/before treatment with DMSO, calcium channel blockers, ROCKi, or MLCK inhibitor. * $p < 0.05$, ** $p < 0.0001$, Fisher exact test. Unless otherwise indicated, inhibitor treatments were not

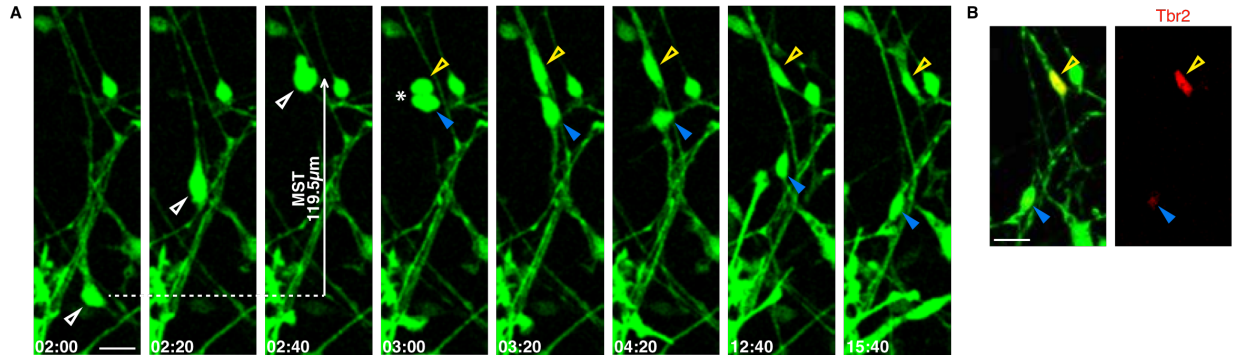
significantly different from DMSO. (B-C) oSVZ sizes and average MST distance in species of analogous gestational ages. (B) Rat and ferret oSVZ measurements are from studies by Martínez-Cerdeño and co-workers (Martinez-Cerdeno 2012). (C) Mouse measurements were re-analyzed from Wang *et al* (Wang 2011) to only include translocation distances of $\geq 20\mu\text{m}$, the definition of MST used in our study. Sample sizes indicated on each column. Error bars, SEM. * $p < .05$. ** $p < .001$, Student's *t* test. (D) Vector plot of MST trajectory angles in human cortical slices ($n=62$ MSTs). Angles grouped in 30° increments, lengths of black arrows represent proportion of MSTs of a given angle, red arrow depicts net MST trajectory (vector sum). (E-F) Fate staining of GW18 human dorsal cortical slices treated with DMSO (E) or $5\mu\text{M}$ blebbistatin (Bleb, F) for 6 days, with BrdU present for the first 24 hours. Approximate boundaries of the oSVZ are indicated. Scalebars, $100\mu\text{m}$. (G) Binning system for quantification of BrdU+ oRG and IP cell distribution. Scalebar, $100\mu\text{m}$, $n=3$ slices per condition. (H) Distribution of Sox2+/BrdU+ oRG cells in DMSO and blebbistatin-treated slices. * $p < 0.01$, ** $p < .0001$, Pearson's chi-squared test. (I) Bin from oSVZ region of a DMSO-treated slice for quantification of Sox2+/BrdU+ oRG cell distribution. Scalebar, $20\mu\text{m}$. (J) Distribution of Tbr2+/BrdU+ IP cells in DMSO and blebbistatin-treated slices. * $p < 0.01$, ** $p < .0001$, Pearson's chi-squared test. (K) Bin from oSVZ region of a DMSO-treated slice for quantification of Tbr2+/BrdU+ IP cell distribution. Scalebar, $20\mu\text{m}$. (L) Proposed molecular pathway controlling MST. Genes associated with human cortical malformations that have previously been demonstrated to regulate specific pathway proteins are shown next to those proteins. MLCP, myosin phosphatase.



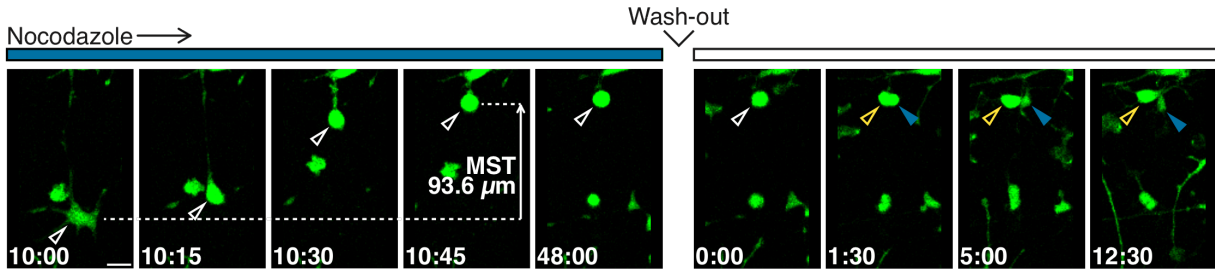
Supplementary Figure S1. Experimental setup. (A) Image of GW16.5 slice labeled with Adeno-GFP, at start of time-lapse imaging. oRG cells are readily identified based on location (oSVZ) and morphology (one long basal process with or without a short apical process). Open white arrowheads indicate examples of oRG cells. Scalebar, 100 μ m. (B) Schematic depicting experimental protocol for treatment of slice culture and dissociated culture with inhibitors. Scalebar, 1cm. (C) Contingency table setup for analysis of mitoses and MSTs before and after treatment with inhibitors.



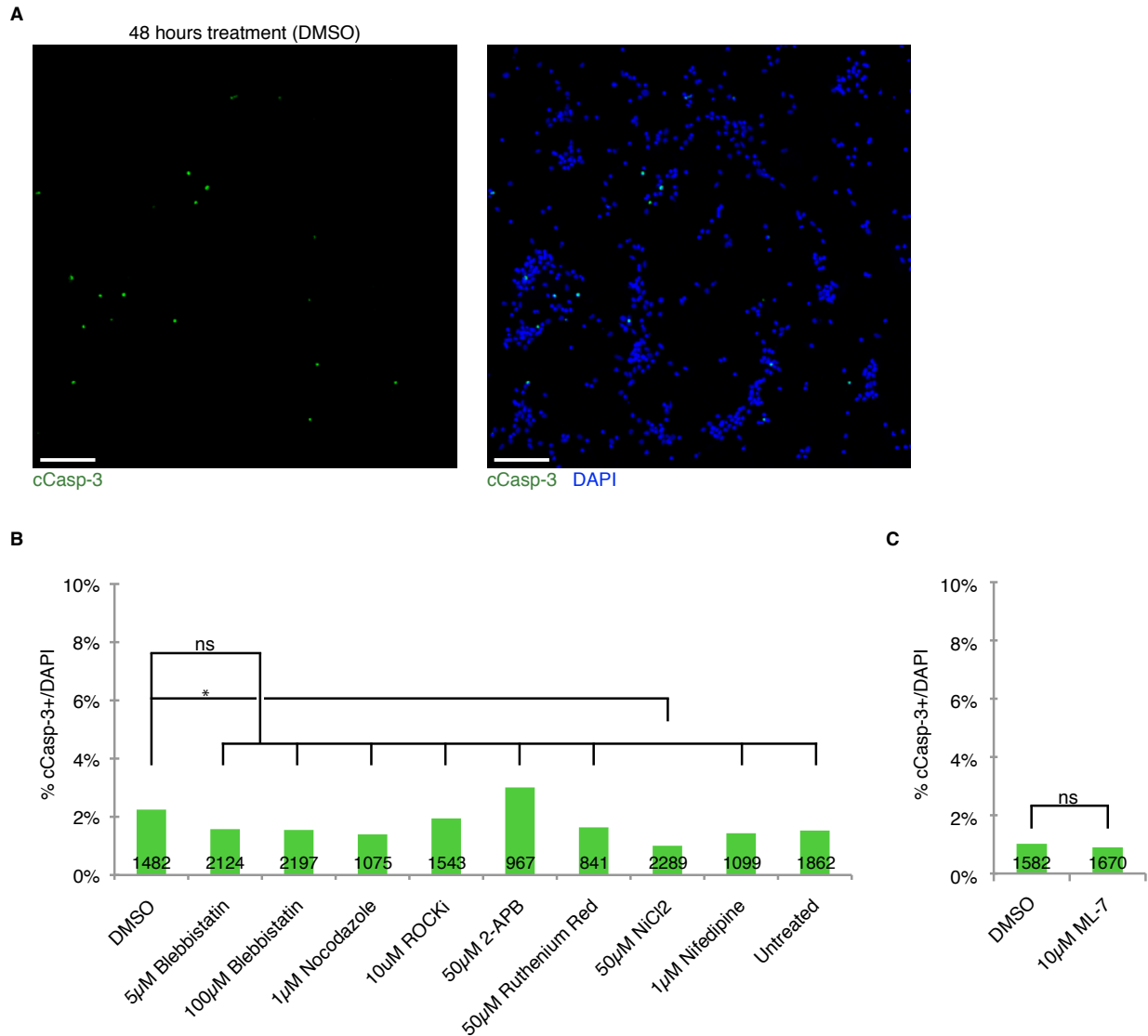
Supplementary Figure S2. Expression of non-muscle myosin II (NMII) in fetal human cortex. (A) GW17.5 dorsal cortex stained for SOX2 (vRG and oRG cells), phosphorylated vimentin (pVim, vRG and oRG cells in mitosis), and NMIIA. NMIIA expression is high in the VZ/iSVZ and oSVZ as compared to the cortical plate, and highest in blood vessels. Scalebar, 200 μ m. (B) GW17.5 dorsal cortex stained for SOX2, pVim, and NMIIB. NMIIB is expressed ubiquitously. Scalebar, 200 μ m.



Supplementary Figure S3. Rare oRG daughters in dissociated culture express Tbr2. (A) Time-lapse stills of oRG cell (open white arrowhead) in GW16.5 dissociated culture labeled with Adeno-GFP. The oRG cell undergoes MST and divides (asterisk) to produce two daughters (open yellow arrowhead and closed blue arrowhead). Time is in hours:minutes. Scalebar, 20 μ m. (B) One oRG daughter demonstrates strong Tbr2 expression (open yellow arrowhead), while the other demonstrates weak Tbr2 expression (closed blue arrowhead). Scalebar, 20 μ m.

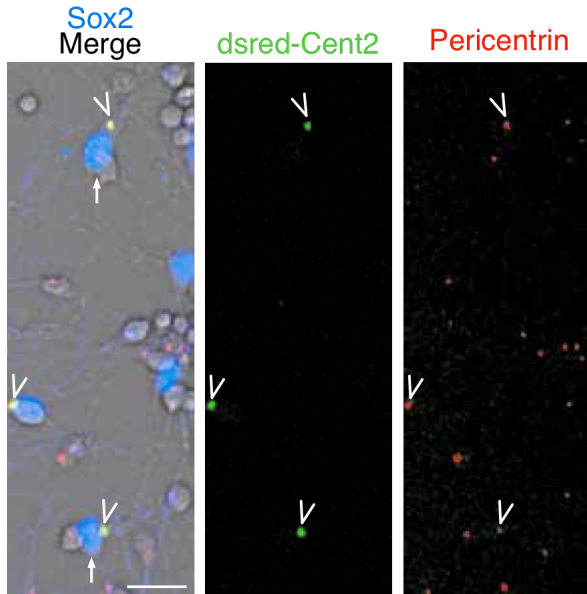


Supplementary Figure S4. Wash-out of nocodazole results in division of oRG cell that previously underwent MST without cytokinesis. Time shown during nocodazole treatment is in hours:minutes since beginning of drug application. Time shown during wash-out is in hours:minutes since replacement with culture medium containing no drugs. The oRG cell (open white arrowhead) undergoes MST ending at 10:45 during nocodazole treatment, but remains rounded up and stalled prior to cytokinesis at the end of the treatment period (48:00). At 1:30 after wash-out, the cell completes mitosis to produce two daughter cells (open yellow arrowhead, closed blue arrowhead). Scalebar, 20μm.

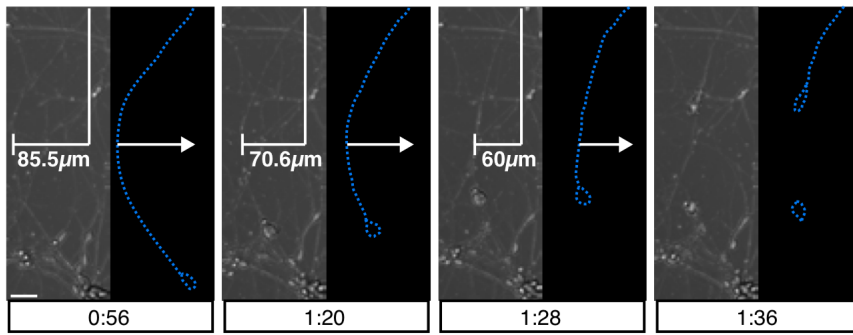


Supplementary Figure S5. Inhibitor treatment does not induce apoptosis. (A) One field of dissociated cells after 48h of DMSO (control) treatment and subsequent staining for cleaved-Caspase 3 (cCasp-3). Approximately 2% of cells are positive for cCasp-3. Scalebar, 100µm. (B) Dissociated cultures were treated with inhibitors of calcium channels and the Rho-ROCK-NMII pathway. Staining for cCasp-3 shows that apoptosis is not increased in inhibitor-treated wells as compared to DMSO. Interestingly, NiCl₂ treatment decreased the proportion of cCasp-3+ cells for unknown reasons. At least two random fields were counted and summed for each condition. Total number of cells counted for each condition is indicated on each column. *p<0.01, Pearson's chi-squared test. (C) Treatment of cultures with myosin

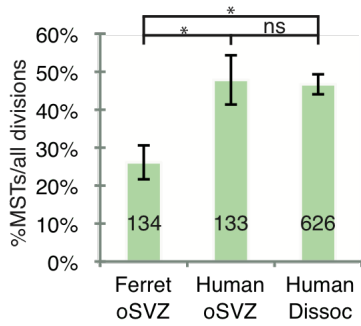
light chain kinase inhibitor ML-7 or DMSO in a separate experiment, followed by cCasp-3 staining. ML-7 did not induce apoptosis above control levels (Pearson's chi-squared test). Total number of cells counted for each condition is indicated on each column.



Supplementary Figure S6. Dsred-Cent2 construct labels centrosomes. Arrows indicate daughter cells from MST division. Arrowheads indicate localization of dsred fluorescence in dissociated cells transfected with dsred-Cent2 construct. Cells were fixed after time-lapse imaging and stained for the centrosome protein pericentrin; colocalization confirms labeling of centrosomes. Scalebar, 20 μ m.

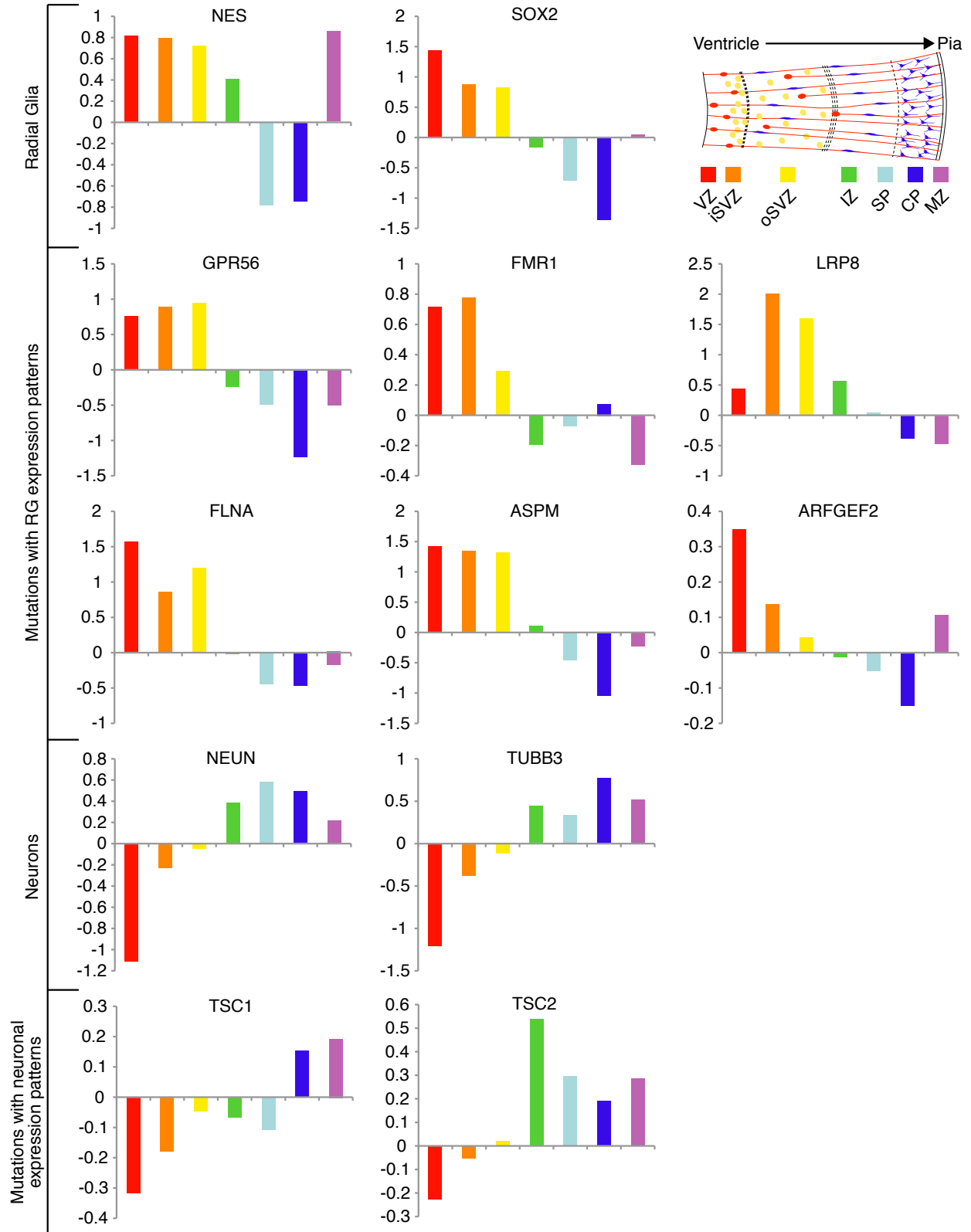


Supplementary Figure S7. oRG basal fiber contraction during MST. Time-lapse stills of human fetal dissociated cortical culture in which an oRG cell with a curved primary fiber undergoes MST. Transmitted light microscopy is shown on left, while outline of the oRG cell and its primary process is depicted on right. Measurements shown in microns depict the decrease in distance during translocation of a single point on the primary fiber from the y-axis of the cell. The entire primary fiber appears to contract prior to and during translocation, suggesting that ROCK-dependent actomyosin contraction in oRG cells occurs throughout the soma and basal process. Scalebar, 30 μ m.



Supplementary Figure S8. Frequency of MST is increased in human as compared to ferret cortex.

Proportion of mitoses preceded by MST in the oSVZ of E39 ferret and GW16.5 human slices and in dissociated human cortical cultures. Total number of divisions analyzed are indicated on each column; n=3 slices for ferret and human oSVZ, n=3 wells for human dissociated cultures. Error bars are SEM. *p<0.01, unpaired Student's *t* test.



Supplementary Figure S9. Expression in germinal zones of the fetal human brain of genes associated with both the RhoA-ROCK-NMII pathway and developmental cortical malformations in humans. Relative mRNA expression levels (y-axis) were obtained from Brainspan from for each gene (BrainSpan). Data were originally generated via laser microdissection and microarray profiling of GW18-23.5 fetal cortical samples. Many candidate genes demonstrate high expression in the VZ, iSVZ, and oSVZ, paralleling known radial glial genes, suggesting a role in radial glial function, such as oRG cell MST. In contrast, the expression profiles of *TSC1* and *TSC2* are more similar to those of known early neuronal markers, suggesting that mutation of these genes may primarily affect neuronal function.

Gene	Relation to RhoA-ROCK-Myosin II Pathway	Human Disease	Mouse Phenotype
<i>ASPM</i>	Controls localization of myosin II (Rujano 2013)	Severe microcephaly (Bond 2002)	Mild microcephaly (Pulvers 2010)
<i>ARFGEF2</i>	Directly interacts with and regulates the phosphorylation of myosin II (Le 2013)	Periventricular heterotopia, microcephaly, simplified gyral pattern (Guerrini 2010)	Early embryonic lethality (Grzmil 2010)
<i>FLNA</i>	Part of ROCK-activated FLNA-FilGAP complex (Nakamura 2013). Activates RhoA, regulates phosphorylation of myosin II (Sun 2013) and <i>ARFGEF2</i> expression/localization (Zhang 2013).	Periventricular Nodular Heterotopia (Guerrini 2010)	Grossly normal brain (Feng 2006)
<i>RELN</i>	Ligand for ApoER2, which activates RhoA (Schmandke 2007)	Lissencephaly (Guerrini 2010)	Cortical layering defects (Guerrini 2010)
<i>FMRI</i>	Regulates translation of RhoA (Davidovic 2011)	Periventricular Heterotopia with Fragile X Syndrome (Guerrini 2010)	No gross or histological brain abnormalities (Bakkar 1994)
<i>TSC1</i>	Regulates RhoA activity (Astrinidis 2002)	Tuberous Sclerosis (cortical tubers) (Guerrini 2010)	Tuber-like brain lesions (Feliciano 2011)
<i>TSC2</i>	same as for <i>TSC1</i>	same as for <i>TSC1</i>	Focal lesions with tuber-like characteristics (Way 2009)
<i>GPR56</i>	Activates RhoA (Singer 2013)	Bilateral frontoparietal polymicrogyria (Singer 2013)	Cortical lamination defects (Singer 2013)

Table S1. Mutations in genes that regulate the RhoA-ROCK-Myosin II pathway. These mutations may disrupt neuronal migration, as previously hypothesized, and also MST due to its dependence on

similar molecular motors. MST may even be the primary target of mutations that have no discernable effects, or minimal or altered phenotypes, when reproduced in mouse models.

METHODS

Fetal tissue collection

Fetal brain tissue was collected from elective pregnancy termination specimens at San Francisco General Hospital, usually within 2 h of the procedure. Gestational age was determined using fetal foot length. Brain tissue was transported in ice-chilled artificial cerebrospinal fluid (ACSF; 125 mM NaCl, 2.5 mM KCl, 1 mM MgCl₂, 2 mM CaCl₂, 1.25 mM NaH₂PO₄, 25 mM NaHCO₃, 25 mM d-(+)-glucose) on ice to the laboratory for further processing. Tissues were collected only with previous patient consent and in strict observance of legal and institutional ethical regulations. Research protocols were approved by the Gamete, Embryo, and Stem Cell Research Committee (institutional review board) at University of California, San Francisco.

Slice culture and real-time imaging

Dorsal cortical tissue obtained from elective pregnancy terminations at gestation week 15-20 (GW15-20), during peak neurogenesis, was processed in ice-chilled ACSF, bubbled with 95% O₂/5% CO₂. Blocks of cortical tissue were trimmed and imbedded in 3-4% low melting point agarose in ACSF. 300- μ m vibratome slices were generated and transferred to cortical slice culture medium (66% BME, 25% Hanks, 5% FBS, 1% N-2, 1% penicillin, streptomycin and glutamine (all Invitrogen) and 0.66% d-(+)-glucose (Sigma)) containing CMV-GFP adenovirus (Vector Biolabs, 1 x 10⁶ c.f.u.), and incubated for 30 minutes at 37 °C, 5% CO₂, 8% O₂. Slices were transferred to and suspended on Millicell-CM slice culture inserts (Millipore) in cortical slice culture medium, and cultured at 37 °C, 5% CO₂, 8% O₂ for ~24 h. Cultures were then transferred to an inverted Leica TCS SP5 with an on-stage incubator (while streaming 5% CO₂, 5% O₂, balanced N₂ into the chamber), and imaged using a x10 or x40 air objective at 15–25-min

intervals for up to 6 days with intermittent repositioning of the focal planes. For inhibitor experiments, at least two positions within the oSVZ of at least two slices for each treatment condition were imaged for 24-48 hours to obtain a "before treatment" number of mitoses and MSTs for each position. Inhibitors or DMSO were then added to each well, and positions were imaged for an equal amount of time as the before treatment period for a given experiment to obtain an "after treatment" number of mitoses and MSTs for each position. Maximum intensity projections of the collected stacks (~30 μm at ~2.5- μm step size) were compiled and generated into movies, which were analyzed using Imaris.

For experiments examining the effects of myosin II inhibition on oSVZ size and distribution of oRG and IP cells (Fig. 4), human fetal cortical slices were made as described above, and transferred to Millicell-CM slice culture inserts within 6-well cell culture plates. Slices were kept in cortical slice culture medium at 37 °C, 5% CO₂, 8% O₂ for 24 h, then cultured for 6 days in similar conditions with cortical slice culture medium containing 0.5% DMSO (control) or 5 μM blebbistatin to inhibit MST. Medium additionally contained BrdU for the first 24h of the 6-day treatment period only. Medium (with inhibitors) was replaced every 24-48h. Slices were fixed for 18h in 4% PFA, and stained for BrdU and expression of IP and oRG markers (see below). To quantify the distribution of newly generated oRG and IP cells, 10 square bins of equal height were spaced evenly between the ventricle and the cortical plate. For every individual slice, the cortical thickness (from ventricle to pial surface) was divided by 20 to determine the height of the bins. For each slice, the number of BrdU+Sox2+ cells ("newly generated oRG cells") were counted in each bin and divided by the total number of BrdU+Sox2+ cells in all 10 bins to determine the fraction of newly generated oRG cells within each bin. The same procedure was performed for BrdU+Tbr2+ cells ("newly generated IP cells"). Data were plotted in vertical histogram format in Fig. 4H and J. Proportions represent the sum of all cell counts in each bin number from 3 slices per condition (DMSO and blebbistatin-treated). The entire experiment was repeated a second time with similar results (data not shown).

Dissociated cortical progenitor culture and real-time imaging

Dorsal cortical tissue was separated from meninges and minced using a razor blade. Cells were dissociated by incubation with papain (Worthington Biochemical Corporation) at 37 °C for 30-40 min followed by addition of DNase I and trituration. Dissociated cells were plated at a density of 500,000-1,000,000 cells per well in 12-well cell culture plates (Greiner Bio-one) pre-coated with matrigel (BD Biosciences). Cultures were maintained in a DMEM-based dissociated culture medium containing 1% N-2, 1% B-27 supplement, 1% penicillin, streptomycin and glutamine (all Invitrogen), sodium pyruvate (0.11mg/mL), 1mM N-acetyl-cysteine, with 10ng/mL hFGF. For cell fate and inhibitor experiments, CMV-GFP adenovirus (Vector Biolabs, 1×10^6 c.f.u.) was applied to cells, which were cultured at 37 °C, 5% CO₂, 8% O₂ until cells demonstrated strong GFP expression (~24h). For centrosome imaging experiments, cells were transfected using jetPRIME reagent (Polyplus) with dsred-Cent2 plasmid (Addgene plasmid 29523), and cultured at 37 °C, 5% CO₂, 8% O₂ until cells demonstrated expression of dsred-Cent2 construct (~24-48h). Cultures were then transferred to an inverted Leica TCS SP5 with an on-stage incubator (while streaming 5% CO₂, 5% O₂, balance N₂ into the chamber), and imaged using a x10 objective at 8-min to 20-min intervals. For inhibitor experiments, two positions per well from at least 2-4 different wells were chosen randomly for each condition. Cells were imaged for 18-48 hours to obtain a "before treatment" number of mitoses and MSTs for each position. Inhibitors or DMSO were then added to each well, and positions were imaged for an equal amount of time as the before treatment period for a given experiment to obtain an "after treatment" number of mitoses and MSTs for each position.

Chemical Inhibitors

Stock solutions of inhibitors were as follows: blebbistatin (100mM in DMSO), nocodazole (2mM in DMSO), NiCl₂ (1M in water), nifedipine (10mM in DMSO), ruthenium red (10mM in DMSO), 2-aminoethoxydiphenyl borate (2-APB) (Sigma, 10mM in DMSO), Y-27632 (10mM in DMSO), and ML-7

(10mM in DMSO). Control treatment was 0.5% DMSO, which was greater than or equal to the final DMSO concentration for each inhibitor. For wash-out experiments, cells were removed from microscope and washed two times with PBS, dissociated culture medium with no drug was replaced, cells were placed back on the microscope, and positions were re-aligned to match previous positions. For cleaved caspase-3 (c-Casp3) staining, dissociated cells were treated with inhibitors for 24-48 hours, fixed with 4% PFA and subjected to immunohistochemistry, and the proportion of cCasp3+/DAPI+ cells in inhibitor-treated wells were compared to proportion of cCasp3+/DAPI+ cells in wells treated with 0.5% DMSO for the same length of time. All movies were analyzed using Imaris.

For initial myosin II and microtubule inhibitor experiments (Figs. 1 and 2), the number of mitoses after/before treatment was as follows: for slices, DMSO: 305/327, blebbistatin: 52/122, nocodazole: 0/254; for dissociated cells, DMSO: 314/463, blebbistatin: 246/450, nocodazole: 0/383. The number of MSTs after/before treatment was as follow: for slices, DMSO: 117/128, blebbistatin: 7/57, nocodazole: 43/118; for dissociated cells: DMSO: 59/95, blebbistatin: 3/98, nocodazole: 49/93. For calcium channel, ROCK, and myosin light chain kinase inhibitor experiments in dissociated cells (Fig. 4), DMSO, NiCl₂, and nifedipine were tested together; number of mitoses after/before treatment was as follows: DMSO: 111/85, NiCl₂: 103/133, nifedipine: 116/93; number of MSTs after/before treatment was as follows: DMSO: 47/40, NiCl₂: 40/40, nifedipine: 51/30. DMSO, ruthenium red (RR), and 2-APB were tested together; number of mitoses after/before treatment was as follows: DMSO: 220/252, RR: 205/190, 2-APB: 134/184; number of MSTs after/before treatment was as follows: DMSO: 95/117; RR: 83/84; 2-APB: 62/91. DMSO and ROCKi were tested together; number of mitoses after/before treatment was as follows: DMSO: 248/281, ROCKi: 274/293; number of MSTs after/before treatment was as follows: DMSO: 105/116. ROCKi: 41/118. DMSO and ML-7 were tested together; number of mitoses after/before treatment was as follows: DMSO: 99/73, ML-7: 93/73; number of MSTs after/before treatment was as follows: DMSO: 29/21. ML-7: 24/23.

Immunohistochemistry

For staining of fetal dorsal cortex, brain tissue was fixed in 4% PFA in PBS at 4 °C for 3 days, dehydrated in 30% sucrose in PBS, embedded and frozen at -80 °C in O.C.T. compound (Tissue-Tek), sectioned on a Leica CM3050S (50 or 20 µm) and stored at -80 °C. Cryosections were subjected to heat/citrate-based antigen retrieval for 10 min and permeabilized and blocked for 3-4 hours in PBS plus 0.1% Triton X-100, 10% serum, 0.2% gelatin. Primary incubations were performed at 4 °C overnight. Washes and secondary incubations were standard procedures. Images were acquired on a Leica TCS SP5 broadband laser confocal microscope. Composite images were automatically stitched upon acquisition using ‘Tilescan’ mode of Leica software. Images with morphological information are maximum intensity projections collected with at least 2-µm *z*-step size. For staining of dissociated cells, time lapse imaging was performed as described above, after which cells were fixed in 4% PFA in PBS for 10 minutes, and washed with PBS. Depending on antigen, cells were subjected to heat/citrate-based antigen retrieval for 0-5 min and permeabilized and blocked for 1 hour in PBS plus 0.1% Triton X-100, 10% serum, 0.2% gelatin. Primary incubations were performed for >1 hr at 24 °C. Washes and secondary incubations were standard procedures. For fate staining of oRG daughters, cells were fixed up to 48h after MST division, and stained as described. For BrdU staining (Fig. 4), slices were fixed in 4% PFA in PBS at 4 °C overnight, and stained as described for cryosections in blocking buffer that contained 0.4% Triton X-100. Staining was performed first for all markers except BrdU, then slices were fixed for an additional hour in 4% PFA, incubated for 1h in 2N HCl at 37°C, incubated for 1h in 0.1M Boric Acid (pH 8.5), and subjected to staining as described for BrdU. Images were acquired on a Leica TCS SP5 broadband laser confocal microscope. All images were analyzed using Imaris.

Primary antibodies were: goat anti-SOX2 (Santa Cruz sc-17320, 1:250), rabbit anti-TBR2 (Millipore AB9618 or Abcam ab23345, 1:400), mouse anti-βIII-tubulin (TUJ1, Covance MMS-435P, 1:250), mouse anti-phospho-vimentin (MBL International D076-3S (Ser 55), 1:500), mouse anti-Ki67 (Dako F7268,

1:150), chicken anti-GFP (Aves Labs GFP-1020, 1:1,000), rabbit anti-nestin (Abcam ab5968, 1:200), rabbit anti-PAX6 (Covance PRB-278P, 1:200), rabbit anti-NMIIa (Covance PRB-440P, 1:500), rabbit anti-NMIIb (Abcam ab24761, 1:400), rat anti-BrdU (Abcam ab6326, 1:100), rabbit anti-active caspase 3 (Promega, 1:250), and rabbit anti-pericentrin (Abcam ab4448, 1:1,000). Secondary antibodies were: AlexaFluor 488 (1:1,000), 546 (1:500), 568 (1:500), 594 (1:500), or 647 (1:500)-conjugated donkey anti-goat, -rabbit or -mouse IgG, or goat anti-chicken IgY (Invitrogen).

Ferret slice culture and real-time imaging

Embryonic day (E) 27 timed-pregnant ferrets were obtained from Marshall BioResources (North Rose, NY) and maintained according to protocols approved by the Institutional Animal Care and Use Committee at the University of California San Francisco. E39 pregnant dams were deeply anesthetized with ketamine followed by isoflurane administration. Ovariohysterectomy for fetus collection was then performed and embryonic brains, along with meninges, removed in ice-chilled ACSF bubbled with 95% O₂/5% CO₂. The dorsal cortex was dissected away from ventral structures, imbedded in 3% low melting point agarose in ACSF, and sectioned using a vibratome to obtain 250-300- μ m slices. Slices were transferred to cortical slice culture medium and treated as described for human slices, including labeling with Adeno-GFP and imaging using an inverted Leica TCS SP5 microscope. Maximum intensity projections of the collected stacks were compiled and generated into movies, which were analyzed using Imaris.

Measurement of MST distances, MST trajectory, and oSVZ size

For quantification of MST distance in human and ferret, MST was defined as a translocation of greater than or equal to 20 μ m (approximately one cell diameter) of the soma along the basal process (slice culture) or the primary process (dissociated culture), with a velocity of greater than or equal to

20 μ m/hour, coinciding with cell rounding, and ending either in immediate cytokinesis or in a prolonged, rounded state. A total of 62 MSTs in 3 aged GW16.5 slices were used for quantification of MST direction. Angle with respect to the ventricular surface was measured, and trajectories were grouped in increments of 30°. A vector sum was computed to determine the overall trajectory of all MSTs. For quantification of oSVZ size in fetal human cortex, fixed brain tissue was dehydrated and cryosectioned as described above. Sections were stained for Ki67, Sox2, and DAPI, and oSVZ size was quantified using Imaris. The boundaries of the oSVZ were defined based on a sparse density of Sox2 and Ki67 staining, and a change in the appearance of nuclei from the iSVZ to the oSVZ visible via DAPI staining.

Microarray Profiling

To examine the expression across brain regions of genes associated with human neurodevelopmental diseases, we used the BrainSpan laser microdissection and microarray profiling dataset made available by the Allen Institute (BrainSpan). The dataset was generated from four brains of ages GW17, 18, 23, and 23.5, which were cryosectioned, microdissected, and subjected to mRNA profiling by hybridization to custom Agilent microarrays. Expression values were normalized in three steps: by sample batch, across all batches of a single brain, and brain by brain. Columns in Figure S9 show the average normalized expression of every value in the dataset from each specified brain region. In the case of multiple probes for a given gene, the expression profile that most closely resembled the expression profile of Sox2 was used.

Statistics

All quantifications were performed blind, and p-values of <0.05 were considered statistically significant. For inhibitor experiments in slices and in dissociated cells, the number of events (mitoses or MSTs) after/before treatment was obtained by dividing the total number of events after treatment in all positions

for a given experiment by the total number of events before treatment in all positions for the same experiment. For each experiment, the number and location of positions was kept constant before and after treatment, and the after treatment and before treatment time intervals lasted up to 48 hours and were always identical in length. The data and graphs in Fig. 2 are the sum of two independent experiments; otherwise, each graph represents one experiment. Ratios were compared pair-wise using either a Fisher's exact test (two-tailed) or a Pearson's chi-squared test, depending on sample size. To calculate the proportion of MSTs resulting in cytokinesis, oRG cells were followed after MST, and were scored as resulting in cytokinesis if cell division occurred before the end of the imaging session. Cells undergoing MST that did not result in cytokinesis remained rounded up after MST and did not divide. In prolonged imaging sessions, cells either died before the end of the imaging session, or remained rounded up for the remainder of the imaging session. Proportions were compared pair-wise using a Fisher's exact test (two-tailed). For comparisons of MST and migratory step translocation distances, and for MST distance comparisons between species, an unpaired Student's *t* test was used. For comparisons between proportions of BrdU+Sox2+ and BrdU+Tbr22+ cells located within each bin in Fig. 4H and J, a Pearson's chi-squared test was used.

CHAPTER 4

Concluding Remarks and Future Work

The incredible expansion and complexity of the human brain arises from developmental processes that we are only beginning to understand. In this thesis, I directly examine the production and proliferation in human fetal cortical tissue of neural stem cells called oRG cells, which are thought to be essential to human neocortical expansion. We find that oRG cells are produced by horizontal division of vRG cells, and that the MST and cleavage angle of oRG cells are cell-intrinsic. We further find that MST is controlled by the Rho-ROCK-myosin pathway, but not by microtubule motors or centrosomal guidance. MST was essential for developmental expansion of the oSVZ, a large germinal zone found in the developing human but not mouse brain. Our findings invite a re-interpretation of the mechanisms behind a wide range of neurodevelopmental diseases, especially those involved in cell motility and migration.

oSVZ evolution and emerging model systems

The presence of progenitor zones and cell types in the developing human but not mouse brain suggests that a complete understanding of human neocortical evolution requires study of both human tissue and more faithful animal models. Following the recent characterization of the human oSVZ, a number of studies have extended these analyses to other species, including ferret and macaque, that share features of human cortical development and may represent potential model systems for exploring disease mechanisms (Fietz 2010; Reillo 2011; Reillo 2011; Wang 2011; Garcia-Moreno 2012; Kelava 2012; Martinez-Cerdeno 2012; Gertz 2014).

The human oSVZ contains the largest proportion of progenitor cells of any species examined so far, but oRG cells are present during development in many species throughout the evolutionary tree (Lui 2011). The amount of oSVZ proliferation appears to correlate with brain size and degree of folding. The lissencephalic brain of mice represents one extreme with no identifiable oSVZ, though recent evidence suggests that the developing rat cortex contains some oSVZ cytoarchitectural features (Martinez-Cerdeno 2012). The ferret brain constitutes an intermediate level of gyrencephaly and oSVZ size, while the highly

folded human cortex sits at the other extreme with a notably developed oSVZ (Lui 2011). This is only a trend and not a rule, however, as the marmoset, a lissencephalic primate, exhibits a large oSVZ containing oRG cells, but may have lost its ancestral gyrencephaly (Garcia-Moreno 2012; Kelava 2012). These findings suggest that oRG cells may be necessary, but not sufficient for developing a large folded brain.

The oSVZ and oRG cells in human disease

We are now in a position to begin applying our expanded knowledge of human brain development to insights about disease mechanisms gained from animal models and from patients with genetic mutations. An increase in the diversity of neural progenitor types between mice and humans invites a reinterpretation of diseases of neurogenesis and cell migration during brain development. How do genetic mutations affect human-specific features of neurodevelopment, including cell populations such as oRG cells, and progenitor zones such as the oSVZ? In this thesis, I show that the Rho-ROCK-myosin pathway is required for MST in oRG cells, and that many disease genes implicated in this pathway cause dramatic cortical malformations in humans but minimal phenotypes in mice. These observations underscore how diseases of cell motility and neuronal migration could have partially or entirely different manifestations in rodent and human. These mutations could affect not just INM and neuronal migration, but also MST and possibly other unidentified novel behaviors required for oSVZ growth. Our observation that several disease genes linked to cortical malformations have an expression profile more similar to oRG cells than neurons suggests that oRG-specific behaviors may even be the primary target in certain diseases.

Similarly, genes important for mitosis, such as centrosome-associated primary microcephaly genes, could be involved in cell division of many different progenitor types. A defect in mitosis of vRG cells suggests the possibility of a similar defect in IP and/or oRG cells; conversely, lack of a phenotype in one progenitor cell type does not preclude a mitosis-related role in a different progenitor cell type. The appreciation that oSVZ progenitor cells could be responsible for generating the majority of cortical

neurons suggests that the oSVZ may be affected in many neurodevelopmental diseases, especially those that broadly affect neuronal number and brain size such as lissencephaly and microcephaly. In the context of the human neocortex, the function of genes implicated in control of mitosis could extend to the oSVZ and specifically to oRG cells, and other newly identified oRG cell subtypes and progeny (Betizeau 2013; Pilz 2013).

Here, we show how a specific pathway (the Rho-ROCK-myosin pathway) linked to neuronal migration disorders controls an essential oRG cell behavior (MST). Future studies will likely reveal that many cellular signaling pathways implicated in neurodevelopmental diseases also function in oRG cells. We must pay special attention to those diseases that have been primarily studied in mouse models, which lack an oSVZ and a significant oRG cell population. Ultimately, our findings highlight the importance of using both animal models and human tissue to attain a comprehensive understanding of human neocortical development, function, and disease.

CHAPTER 5

References

Alkuraya, F. S., X. Cai, et al. (2011). "Human mutations in NDE1 cause extreme microcephaly with lissencephaly [corrected]." Am J Hum Genet **88**(5): 536-47.

Astrinidis, A., T. P. Cash, et al. (2002). "Tuberin, the tuberous sclerosis complex 2 tumor suppressor gene product, regulates Rho activation, cell adhesion and migration." Oncogene **21**(55): 8470-6.

Bai, J., R. L. Ramos, et al. (2003). "RNAi reveals doublecortin is required for radial migration in rat neocortex." Nat Neurosci **6**(12): 1277-83.

Bakircioglu, M., O. P. Carvalho, et al. (2011). "The essential role of centrosomal NDE1 in human cerebral cortex neurogenesis." Am J Hum Genet **88**(5): 523-35.

Bakkar, C. E., C. Verheij, et al. (1994). "Fmr1 knockout mice: a model to study fragile X mental retardation. The Dutch-Belgian Fragile X Consortium." Cell **78**(1): 23-33.

Barrera, J. A., L. R. Kao, et al. (2010). "CDK5RAP2 regulates centriole engagement and cohesion in mice." Dev Cell **18**(6): 913-26.

Bentivoglio, M. and P. Mazzarello (1999). "The history of radial glia." Brain Res Bull **49**(5): 305-15.

Betizeau, M., V. Cortay, et al. (2013). "Precursor diversity and complexity of lineage relationships in the outer subventricular zone of the primate." Neuron **80**(2): 442-57.

Bhat, V., S. C. Girimaji, et al. (2011). "Mutations in WDR62, encoding a centrosomal and nuclear protein, in Indian primary microcephaly families with cortical malformations." Clin Genet **80**(6): 532-40.

Bond, J., E. Roberts, et al. (2002). "ASPM is a major determinant of cerebral cortical size." Nat Genet **32**(2): 316-20.

Bond, J., E. Roberts, et al. (2005). "A centrosomal mechanism involving CDK5RAP2 and CENPJ controls brain size." Nat Genet **37**(4): 353-5.

BrainSpan: Atlas of the Developing Human Brain [Internet]. Funded by ARRA Awards 1RC2MH089921-01, 1RC2MH090047-01, and 1RC2MH089929-01. © 2011. Available from: <http://developinghumanbrain.org>.

Buchman, J. J., H. C. Tseng, et al. (2010). "Cdk5rap2 interacts with pericentrin to maintain the neural progenitor pool in the developing neocortex." Neuron **66**(3): 386-402.

Bultje, R. S., D. R. Castaneda-Castellanos, et al. (2009). "Mammalian Par3 regulates progenitor cell asymmetric division via notch signaling in the developing neocortex." Neuron **63**(2): 189-202.

Campos, L. S., A. J. Duarte, et al. (2001). "mDil1 and mDil3 expression in the developing mouse brain: role in the establishment of the early cortex." J Neurosci Res **64**(6): 590-8.

Chenn, A. and S. K. McConnell (1995). "Cleavage orientation and the asymmetric inheritance of Notch1 immunoreactivity in mammalian neurogenesis." Cell **82**(4): 631-41.

Chenn, A., Y. A. Zhang, et al. (1998). "Intrinsic polarity of mammalian neuroepithelial cells." Mol Cell Neurosci **11**(4): 183-93.

Chia, W., W. G. Somers, et al. (2008). "Drosophila neuroblast asymmetric divisions: cell cycle regulators, asymmetric protein localization, and tumorigenesis." J Cell Biol **180**(2): 267-72.

Choi, Y. K., P. Liu, et al. (2010). "CDK5RAP2 stimulates microtubule nucleation by the gamma-tubulin ring complex." J Cell Biol **191**(6): 1089-95.

Curchoe, C. L., J. Russo, et al. (2012). "hESC derived neuro-epithelial rosettes recapitulate early mammalian neurulation events; an in vitro model." Stem Cell Res **8**(2): 239-46.

Davidovic, L., V. Navratil, et al. (2011). "A metabolomic and systems biology perspective on the brain of the fragile X syndrome mouse model." Genome Res **21**(12): 2190-202.

Doxsey, S., D. McCollum, et al. (2005). "Centrosomes in cellular regulation." Annu Rev Cell Dev Biol **21**: 411-34.

Feliciano, D. M., T. Su, et al. (2011). "Single-cell Tsc1 knockout during corticogenesis generates tuber-like lesions and reduces seizure threshold in mice." J Clin Invest **121**(4): 1596-607.

Feng, Y., M. H. Chen, et al. (2006). "Filamin A (FLNA) is required for cell-cell contact in vascular development and cardiac morphogenesis." Proc Natl Acad Sci U S A **103**(52): 19836-41.

Feng, Y. and C. A. Walsh (2004). "Mitotic spindle regulation by Nde1 controls cerebral cortical size." Neuron **44**(2): 279-93.

Fietz, S. A. and W. B. Huttner (2011). "Cortical progenitor expansion, self-renewal and neurogenesis-a polarized perspective." Curr Opin Neurobiol **21**(1): 23-35.

Fietz, S. A., I. Kelava, et al. (2010). "OSVZ progenitors of human and ferret neocortex are epithelial-like and expand by integrin signaling." Nat Neurosci **13**(6): 690-9.

Fish, J. L., Y. Kosodo, et al. (2006). "Aspm specifically maintains symmetric proliferative divisions of neuroepithelial cells." Proc Natl Acad Sci U S A **103**(27): 10438-43.

Gaiano, N., J. S. Nye, et al. (2000). "Radial glial identity is promoted by Notch1 signaling in the murine forebrain." Neuron **26**(2): 395-404.

Gal, J. S., Y. M. Morozov, et al. (2006). "Molecular and morphological heterogeneity of neural precursors in the mouse neocortical proliferative zones." J Neurosci **26**(3): 1045-56.

Garcia-Moreno, F., N. A. Vasistha, et al. (2012). "Compartmentalization of cerebral cortical germinal zones in a lissencephalic primate and gyrencephalic rodent." Cereb Cortex **22**(2): 482-92.

Gertz, C. C., J. H. Lui, et al. (2014). "Diverse behaviors of outer radial glia in developing ferret and human cortex." J Neurosci **34**(7): 2559-70.

Ghannad, M. (2011). "The essential role of NDE1 in extreme microcephaly." Clin Genet **80**(3): 241-2.

Govek, E. E., M. E. Hatten, et al. (2011). "The role of Rho GTPase proteins in CNS neuronal migration." Dev Neurobiol **71**(6): 528-53.

Gruber, R., Z. Zhou, et al. (2011). "MCPH1 regulates the neuroprogenitor division mode by coupling the centrosomal cycle with mitotic entry through the Chk1-Cdc25 pathway." Nat Cell Biol **13**(11): 1325-34.

Grzmil, P., Z. Enkhbaatar, et al. (2010). "Early embryonic lethality in gene trap mice with disruption of the Arfgef2 gene." Int J Dev Biol **54**(8-9): 1259-66.

Guan, C. B., H. T. Xu, et al. (2007). "Long-range Ca²⁺ signaling from growth cone to soma mediates reversal of neuronal migration induced by slit-2." Cell **129**(2): 385-95.

Guernsey, D. L., H. Jiang, et al. (2010). "Mutations in centrosomal protein CEP152 in primary microcephaly families linked to MCPH4." Am J Hum Genet **87**(1): 40-51.

Guerrini, R. and E. Parrini (2010). "Neuronal migration disorders." Neurobiol Dis **38**(2): 154-66.

Hansen, D. V., J. H. Lui, et al. (2010). "Neurogenic radial glia in the outer subventricular zone of human neocortex." Nature **464**(7288): 554-561.

Hartfuss, E., R. Galli, et al. (2001). "Characterization of CNS precursor subtypes and radial glia." Dev Biol **229**(1): 15-30.

Haubensak, W., A. Attardo, et al. (2004). "Neurons arise in the basal neuroepithelium of the early mammalian telencephalon: a major site of neurogenesis." Proc Natl Acad Sci U S A **101**(9): 3196-201.

Haubst, N., E. Georges-Labouesse, et al. (2006). "Basement membrane attachment is dispensable for radial glial cell fate and for proliferation, but affects positioning of neuronal subtypes." Development **133**(16): 3245-54.

Heng, Y. W. and C. G. Koh (2010). "Actin cytoskeleton dynamics and the cell division cycle." Int J Biochem Cell Biol **42**(10): 1622-33.

Hevner, R. F. and T. F. Haydar (2012). "The (not necessarily) convoluted role of basal radial glia in cortical neurogenesis." Cereb Cortex **22**(2): 465-8.

Higgins, J., C. Midgley, et al. (2010). "Human ASPM participates in spindle organisation, spindle orientation and cytokinesis." BMC Cell Biol **11**: 85.

Hinds, J. W. and T. L. Ruffett (1971). "Cell proliferation in the neural tube: an electron microscopic and golgi analysis in the mouse cerebral vesicle." Z Zellforsch Mikrosk Anat **115**(2): 226-64.

Hockfield, S. and R. D. McKay (1985). "Identification of major cell classes in the developing mammalian nervous system." J Neurosci **5**(12): 3310-28.

Howard, B., Y. Chen, et al. (2006). "Cortical progenitor cells in the developing human telencephalon." Glia **53**(1): 57-66.

Huang, Z. (2009). "Molecular regulation of neuronal migration during neocortical development." Mol Cell Neurosci **42**(1): 11-22.

Jackson, A. P., H. Eastwood, et al. (2002). "Identification of microcephalin, a protein implicated in determining the size of the human brain." Am J Hum Genet **71**(1): 136-42.

Jackson, A. P., D. P. McHale, et al. (1998). "Primary autosomal recessive microcephaly (MCPH1) maps to chromosome 8p22-pter." Am J Hum Genet **63**(2): 541-6.

Kaindl, A. M., S. Passemard, et al. (2009). "Many roads lead to primary autosomal recessive microcephaly." Prog Neurobiol **90**(3): 363-83.

Kamei, Y., N. Inagaki, et al. (1998). "Visualization of mitotic radial glial lineage cells in the developing rat brain by Cdc2 kinase-phosphorylated vimentin." Glia **23**(3): 191-9.

Keays, D. A., G. Tian, et al. (2007). "Mutations in alpha-tubulin cause abnormal neuronal migration in mice and lissencephaly in humans." Cell **128**(1): 45-57.

Kelava, I., I. Reillo, et al. (2012). "Abundant Occurrence of Basal Radial Glia in the Subventricular Zone of Embryonic Neocortex of a Lissencephalic Primate, the Common Marmoset *Callithrix jacchus*." Cereb Cortex **22**(2): 469-81.

Kitagawa, D., G. Kohlmaier, et al. (2011). "Spindle positioning in human cells relies on proper centriole formation and on the microcephaly proteins CPAP and STIL." J Cell Sci **124**(Pt 22): 3884-93.

Koizumi, H., H. Higginbotham, et al. (2006). "Doublecortin maintains bipolar shape and nuclear translocation during migration in the adult forebrain." Nat Neurosci **9**(6): 779-86.

Komuro, H. and P. Rakic (1992). "Selective role of N-type calcium channels in neuronal migration." Science **257**(5071): 806-9.

Kosodo, Y., T. Suetsugu, et al. (2011). "Regulation of interkinetic nuclear migration by cell cycle-coupled active and passive mechanisms in the developing brain." EMBO J **30**(9): 1690-704.

Kouprina, N., A. Pavlicek, et al. (2005). "The microcephaly ASPM gene is expressed in proliferating tissues and encodes for a mitotic spindle protein." Hum Mol Genet **14**(15): 2155-65.

Kriegstein, A. and A. Alvarez-Buylla (2009). "The glial nature of embryonic and adult neural stem cells." Annu Rev Neurosci **32**: 149-84.

Kumar, A., S. C. Girimaji, et al. (2009). "Mutations in STIL, encoding a pericentriolar and centrosomal protein, cause primary microcephaly." Am J Hum Genet **84**(2): 286-90.

Kusek, G., M. Campbell, et al. (2012). "Asymmetric Segregation of the Double-Stranded RNA Binding Protein Staufen2 during Mammalian Neural Stem Cell Divisions Promotes Lineage Progression." Cell Stem Cell.

LaMonica, B. E., J. H. Lui, et al. (2013). "Mitotic spindle orientation predicts outer radial glial cell generation in human neocortex." Nat Commun **4**: 1665.

LaMonica, B. E., J. H. Lui, et al. (2012). "OSVZ progenitors in the human cortex: an updated perspective on neurodevelopmental disease." Curr Opin Neurobiol.

Lancaster, M. A. and J. A. Knoblich (2012). "Spindle orientation in mammalian cerebral cortical development." Curr Opin Neurobiol.

Landrieu, P. and A. Goffinet (1979). "Mitotic spindle fiber orientation in relation to cell migration in the neo-cortex of normal and reeler mouse." Neurosci Lett **13**(1): 69-72.

Le, K., C. C. Li, et al. (2013). "Arf guanine nucleotide-exchange factors BIG1 and BIG2 regulate nonmuscle myosin IIA activity by anchoring myosin phosphatase complex." Proc Natl Acad Sci U S A **110**(34): E3162-70.

Leal, G. F., E. Roberts, et al. (2003). "A novel locus for autosomal recessive primary microcephaly (MCPH6) maps to 13q12.2." J Med Genet **40**(7): 540-2.

Lizarraga, S. B., S. P. Margossian, et al. (2010). "Cdk5rap2 regulates centrosome function and chromosome segregation in neuronal progenitors." Development **137**(11): 1907-17.

Lui, J. H., D. V. Hansen, et al. (2011). "Development and evolution of the human neocortex." Cell **146**(1): 18-36.

Malatesta, P., E. Hartfuss, et al. (2000). "Isolation of radial glial cells by fluorescent-activated cell sorting reveals a neuronal lineage." Development **127**(24): 5253-63.

Mansson, A. (2012). "Translational actomyosin research: fundamental insights and applications hand in hand." J Muscle Res Cell Motil **33**(3-4): 219-33.

Manzini, M. C. and C. A. Walsh (2011). "What disorders of cortical development tell us about the cortex: one plus one does not always make two." Curr Opin Genet Dev **21**(3): 333-9.

Martinez-Cerdeno, V., C. L. Cunningham, et al. (2012). "Comparative analysis of the subventricular zone in rat, ferret and macaque: evidence for an outer subventricular zone in rodents." PLoS One **7**(1): e30178.

Megraw, T. L., J. T. Sharkey, et al. (2011). "Cdk5rap2 exposes the centrosomal root of microcephaly syndromes." Trends Cell Biol **21**(8): 470-80.

Minobe, S., A. Sakakibara, et al. (2009). "Rac is involved in the interkinetic nuclear migration of cortical progenitor cells." Neurosci Res **63**(4): 294-301.

Misson, J. P., C. P. Austin, et al. (1991). "The alignment of migrating neural cells in relation to the murine neopallial radial glial fiber system." Cereb Cortex **1**(3): 221-9.

Miyata, T., A. Kawaguchi, et al. (2001). "Asymmetric inheritance of radial glial fibers by cortical neurons." Neuron **31**(5): 727-41.

Miyata, T., A. Kawaguchi, et al. (2004). "Asymmetric production of surface-dividing and non-surface-dividing cortical progenitor cells." Development **131**(13): 3133-45.

Moynihan, L., A. P. Jackson, et al. (2000). "A third novel locus for primary autosomal recessive microcephaly maps to chromosome 9q34." Am J Hum Genet **66**(2): 724-7.

Nakamura, F. (2013). "FilGAP and its close relatives: a mediator of Rho-Rac antagonism that regulates cell morphology and migration." Biochem J **453**(1): 17-25.

Noctor, G., C. Dutilleul, et al. (2004). "Use of mitochondrial electron transport mutants to evaluate the effects of redox state on photosynthesis, stress tolerance and the integration of carbon/nitrogen metabolism." J Exp Bot **55**(394): 49-57.

Noctor, S. C., A. C. Flint, et al. (2001). "Neurons derived from radial glial cells establish radial units in neocortex." Nature **409**(6821): 714-20.

Noctor, S. C., V. Martinez-Cerdeno, et al. (2004). "Cortical neurons arise in symmetric and asymmetric division zones and migrate through specific phases." Nat Neurosci **7**(2): 136-44.

Noctor, S. C., V. Martinez-Cerdeno, et al. (2008). "Distinct behaviors of neural stem and progenitor cells underlie cortical neurogenesis." J Comp Neurol **508**(1): 28-44.

Norden, C., S. Young, et al. (2009). "Actomyosin is the main driver of interkinetic nuclear migration in the retina." Cell **138**(6): 1195-208.

Pattison, L., Y. J. Crow, et al. (2000). "A fifth locus for primary autosomal recessive microcephaly maps to chromosome 1q31." Am J Hum Genet **67**(6): 1578-80.

Peyre, E. and X. Morin (2012). "An oblique view on the role of spindle orientation in vertebrate neurogenesis." Dev Growth Differ **54**(3): 287-305.

Pilz, G. A., A. Shitamukai, et al. (2013). "Amplification of progenitors in the mammalian telencephalon includes a new radial glial cell type." Nat Commun **4**: 2125.

Pixley, S. K. and J. de Vellis (1984). "Transition between immature radial glia and mature astrocytes studied with a monoclonal antibody to vimentin." Brain Res **317**(2): 201-9.

Pulvers, J. N., J. Bryk, et al. (2010). "Mutations in mouse *Aspm* (abnormal spindle-like microcephaly associated) cause not only microcephaly but also major defects in the germline." Proc Natl Acad Sci U S A **107**(38): 16595-600.

Qian, X., S. K. Goderie, et al. (1998). "Intrinsic programs of patterned cell lineages in isolated vertebrate CNS ventricular zone cells." Development **125**(16): 3143-52.

Rakic, P. (1971). "Guidance of neurons migrating to the fetal monkey neocortex." Brain Res **33**(2): 471-6.

Rakic, P. (1972). "Mode of cell migration to the superficial layers of fetal monkey neocortex." J Comp Neurol **145**(1): 61-83.

Rasin, M. R., V. R. Gazula, et al. (2007). "Numb and Numbl are required for maintenance of cadherin-based adhesion and polarity of neural progenitors." Nat Neurosci **10**(7): 819-27.

Rauch, A., C. T. Thiel, et al. (2008). "Mutations in the pericentrin (PCNT) gene cause primordial dwarfism." Science **319**(5864): 816-9.

Reillo, I. and V. Borrell (2011). "Germinal Zones in the Developing Cerebral Cortex of Ferret: Ontogeny, Cell Cycle Kinetics, and Diversity of Progenitors." Cereb Cortex.

Reillo, I., C. de Juan Romero, et al. (2011). "A role for intermediate radial glia in the tangential expansion of the mammalian cerebral cortex." Cereb Cortex **21**(7): 1674-94.

Rujano, M. A., L. Sanchez-Pulido, et al. (2013). "The microcephaly protein *Asp* regulates neuroepithelium morphogenesis by controlling the spatial distribution of myosin II." Nat Cell Biol **15**(11): 1294-306.

Rusan, N. M., U. S. Tulu, et al. (2002). "Reorganization of the microtubule array in prophase/prometaphase requires cytoplasmic dynein-dependent microtubule transport." J Cell Biol **158**(6): 997-1003.

Schaar, B. T. and S. K. McConnell (2005). "Cytoskeletal coordination during neuronal migration." Proc Natl Acad Sci U S A **102**(38): 13652-7.

Schenk, J., M. Wilsch-Brauninger, et al. (2009). "Myosin II is required for interkinetic nuclear migration of neural progenitors." Proc Natl Acad Sci U S A **106**(38): 16487-92.

Schmandke, A. and S. M. Strittmatter (2007). "ROCK and Rho: biochemistry and neuronal functions of Rho-associated protein kinases." Neuroscientist **13**(5): 454-69.

Shen, J., W. Eyaid, et al. (2005). "ASPM mutations identified in patients with primary microcephaly and seizures." J Med Genet **42**(9): 725-9.

Shen, Q., W. Zhong, et al. (2002). "Asymmetric Numb distribution is critical for asymmetric cell division of mouse cerebral cortical stem cells and neuroblasts." Development **129**(20): 4843-53.

Shinohara, R., D. Thumkeo, et al. (2012). "A role for mDia, a Rho-regulated actin nucleator, in tangential migration of interneuron precursors." Nat Neurosci **15**(3): 373-80, S1-2.

Shitamukai, A., D. Konno, et al. (2011). "Oblique radial glial divisions in the developing mouse neocortex induce self-renewing progenitors outside the germinal zone that resemble primate outer subventricular zone progenitors." J Neurosci **31**(10): 3683-95.

Siegenthaler, J. A., A. M. Ashique, et al. (2009). "Retinoic acid from the meninges regulates cortical neuron generation." Cell **139**(3): 597-609.

Singer, K., R. Luo, et al. (2013). "GPR56 and the developing cerebral cortex: cells, matrix, and neuronal migration." Mol Neurobiol **47**(1): 186-96.

Smart, I. H. (1973). "Proliferative characteristics of the ependymal layer during the early development of the mouse neocortex: a pilot study based on recording the number, location and plane of cleavage of mitotic figures." J Anat **116**(Pt 1): 67-91.

Smart, I. H., C. Dehay, et al. (2002). "Unique morphological features of the proliferative zones and postmitotic compartments of the neural epithelium giving rise to striate and extrastriate cortex in the monkey." Cereb Cortex **12**(1): 37-53.

Stancik, E. K., I. Navarro-Quiroga, et al. (2010). "Heterogeneity in ventricular zone neural precursors contributes to neuronal fate diversity in the postnatal neocortex." J Neurosci **30**(20): 7028-36.

- Sun, C., C. Forster, et al. (2013). "Filamin-A Regulates Neutrophil Uropod Retraction through RhoA during Chemotaxis." PLoS One **8**(10): e79009.
- Tanaka, T., F. F. Serneo, et al. (2004). "Lis1 and doublecortin function with dynein to mediate coupling of the nucleus to the centrosome in neuronal migration." J Cell Biol **165**(5): 709-21.
- Taverna, E. and W. B. Huttner (2010). "Neural progenitor nuclei IN motion." Neuron **67**(6): 906-14.
- Tischfield, M. A., G. Y. Cederquist, et al. (2011). "Phenotypic spectrum of the tubulin-related disorders and functional implications of disease-causing mutations." Curr Opin Genet Dev **21**(3): 286-94.
- Tsai, J. W., K. H. Bremner, et al. (2007). "Dual subcellular roles for LIS1 and dynein in radial neuronal migration in live brain tissue." Nat Neurosci **10**(8): 970-9.
- Tsai, J. W., W. N. Lian, et al. (2010). "Kinesin 3 and cytoplasmic dynein mediate interkinetic nuclear migration in neural stem cells." Nat Neurosci **13**(12): 1463-71.
- Tullio, A. N., P. C. Bridgman, et al. (2001). "Structural abnormalities develop in the brain after ablation of the gene encoding nonmuscle myosin II-B heavy chain." J Comp Neurol **433**(1): 62-74.
- Vallee, R. B., G. E. Seale, et al. (2009). "Emerging roles for myosin II and cytoplasmic dynein in migrating neurons and growth cones." Trends Cell Biol **19**(7): 347-55.
- Vicente-Manzanares, M., X. Ma, et al. (2009). "Non-muscle myosin II takes centre stage in cell adhesion and migration." Nat Rev Mol Cell Biol **10**(11): 778-90.
- Wang, X., J. W. Tsai, et al. (2009). "Asymmetric centrosome inheritance maintains neural progenitors in the neocortex." Nature **461**(7266): 947-55.
- Wang, X., J. W. Tsai, et al. (2011). "A new subtype of progenitor cell in the mouse embryonic neocortex." Nat Neurosci **14**(5): 555-61.
- Way, S. W., J. McKenna, 3rd, et al. (2009). "Loss of Tsc2 in radial glia models the brain pathology of tuberous sclerosis complex in the mouse." Hum Mol Genet **18**(7): 1252-65.
- Weissman, T., S. C. Noctor, et al. (2003). "Neurogenic radial glial cells in reptile, rodent and human: from mitosis to migration." Cereb Cortex **13**(6): 550-9.

Yamashita, Y. M., A. P. Mahowald, et al. (2007). "Asymmetric inheritance of mother versus daughter centrosome in stem cell division." Science **315**(5811): 518-21.

Yingling, J., Y. H. Youn, et al. (2008). "Neuroepithelial stem cell proliferation requires LIS1 for precise spindle orientation and symmetric division." Cell **132**(3): 474-86.

Zamenhof, S. (1987). "Quantitative studies of mitoses in fetal rat brain: orientations of the spindles." Brain Res **428**(1): 143-6.

Zecevic, N. (2004). "Specific characteristic of radial glia in the human fetal telencephalon." Glia **48**(1): 27-35.

Zecevic, N., Y. Chen, et al. (2005). "Contributions of cortical subventricular zone to the development of the human cerebral cortex." J Comp Neurol **491**(2): 109-22.

Zhang, J., J. Neal, et al. (2013). "Filamin A regulates neuronal migration through brefeldin A-inhibited guanine exchange factor 2-dependent Arf1 activation." J Neurosci **33**(40): 15735-46.

Zhang, J., G. J. Woodhead, et al. (2010). "Cortical neural precursors inhibit their own differentiation via N-cadherin maintenance of beta-catenin signaling." Dev Cell **18**(3): 472-9.

Zhong, W., J. N. Feder, et al. (1996). "Asymmetric localization of a mammalian numb homolog during mouse cortical neurogenesis." Neuron **17**(1): 43-53.

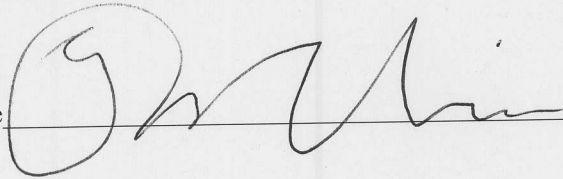
Zimmerman, W. C., J. Sillibourne, et al. (2004). "Mitosis-specific anchoring of gamma tubulin complexes by pericentrin controls spindle organization and mitotic entry." Mol Biol Cell **15**(8): 3642-57.

PUBLISHING AGREEMENT

It is the policy of the University to encourage the distribution of all theses, dissertations, and manuscripts. Copies of all UCSF theses, dissertations, and manuscripts will be routed to the library via the Graduate Division. The library will make all theses, dissertations, and manuscripts accessible to the public and will preserve these to the best of their abilities, in perpetuity.

I hereby grant permission to the Graduate Division of the University of California, San Francisco to release copies of my thesis, dissertation, or manuscript to the Campus Library to provide access and preservation, in whole or in part, in perpetuity.

Author Signature



Date

3/21/2014